Synergetic Spin Singlet-Quintet Switching and Luminescence in mononuclear Fe(II) 1,3,4-Oxadiazole Tetradentate Chelates with $NCBH_3$ Co-ligand.

Sriram Sundaresan,[a] Jens-Georg Becker,[a] Julian Eppelsheimer,[a] Alexander Sedykh,[b] Luca. M. Carrella,[a] Müller-Buschbaum[b] and Eva Rentschler[a*]

[a]Department Chemie, Johannes-Gutenberg-Universität Mainz, Duesbergweg 10–14, 55128 Mainz, Germany. Email: rentschl@uni-mainz.de
[b]Institute of Inorganic and Analytical Chemistry, Justus-Liebig-University Giessen, Heinrich-Buff-Ring 17, 35392, Giessen, Germany.

Electronic Supplementary Information

Table of Contents

1. NMR-spectra: 2
2. IR-spectra: 10
3. Mass spectra: 12
4. Crystal structures: 14
5. UV-Vis-Spectra: 18
6. Photoluminescence spectroscopy 20
6. Magnetic Data: 22
7. Synthesis of complex precursors 25
8. References: 25

1. NMR-spectra:

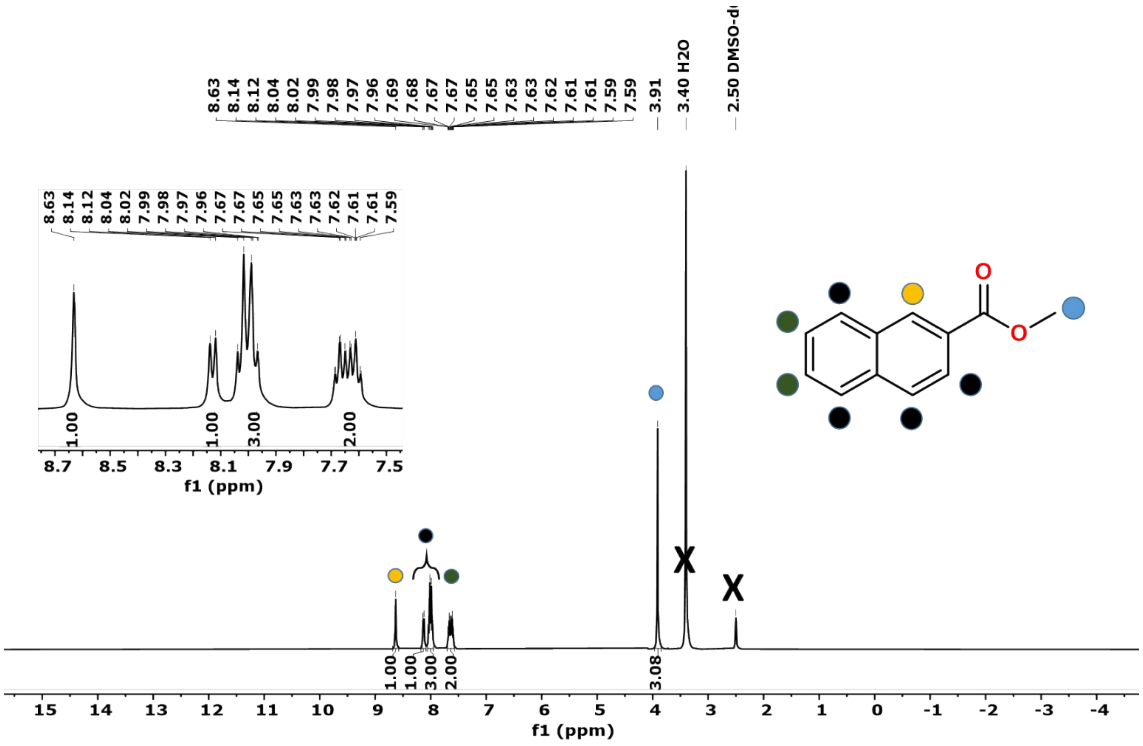

Figure S1: ^{1}H-NMR-spectra of Methyl-2-naphthoate (**I**) in D^{6}-DMSO.

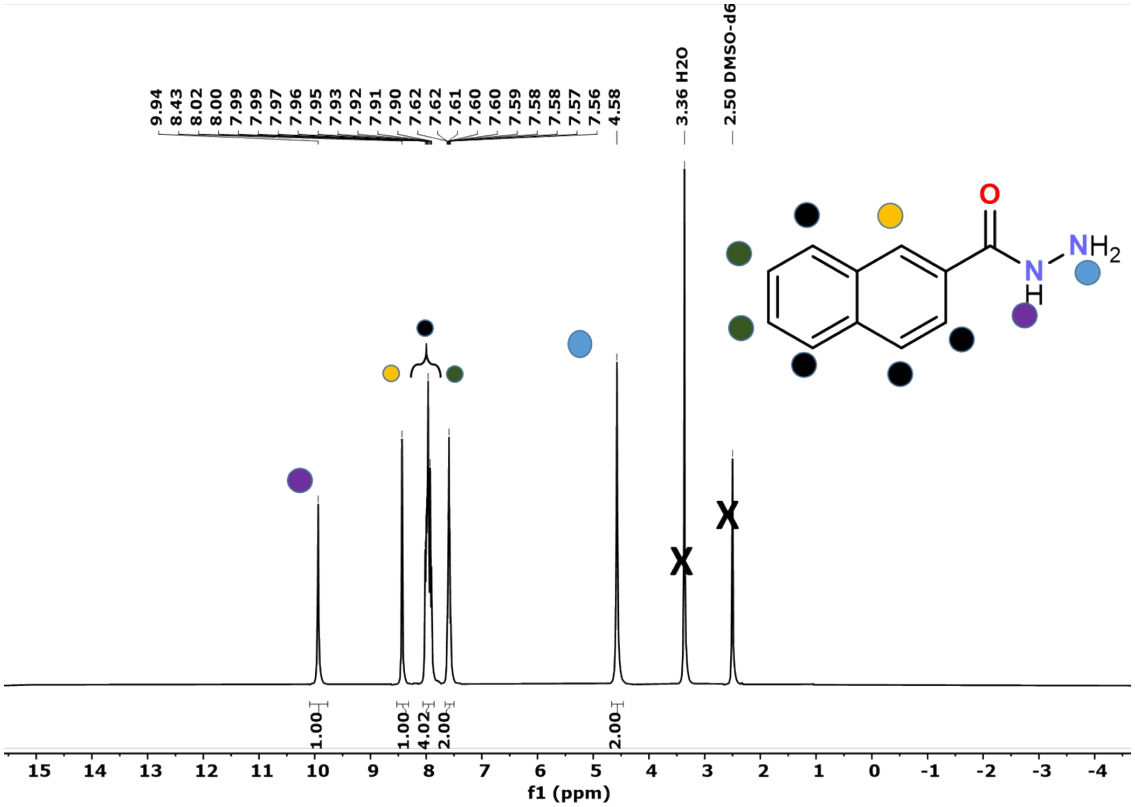

Figure S2: ^{1}H-NMR-spectra of 2-Naphthohydrazide (**II**) in D^{6}-DMSO.

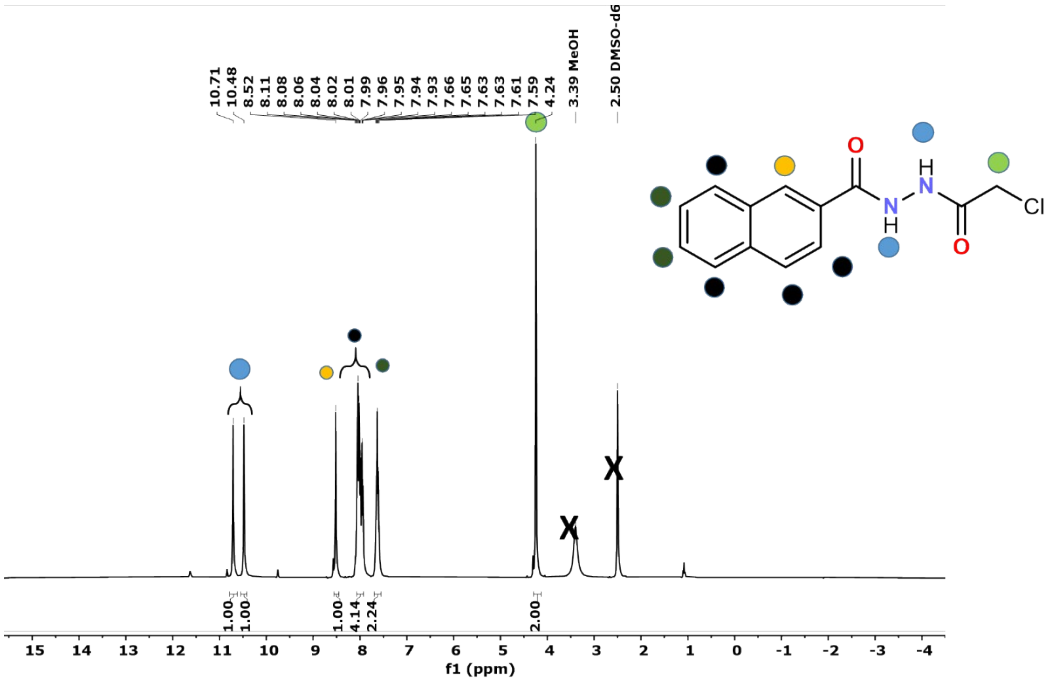

Figure S3: ^{1}H-NMR-spectra of N'-(2-chloroacetyl)-2-naphthohydrazide (**III**) in D^{6}-DMSO.

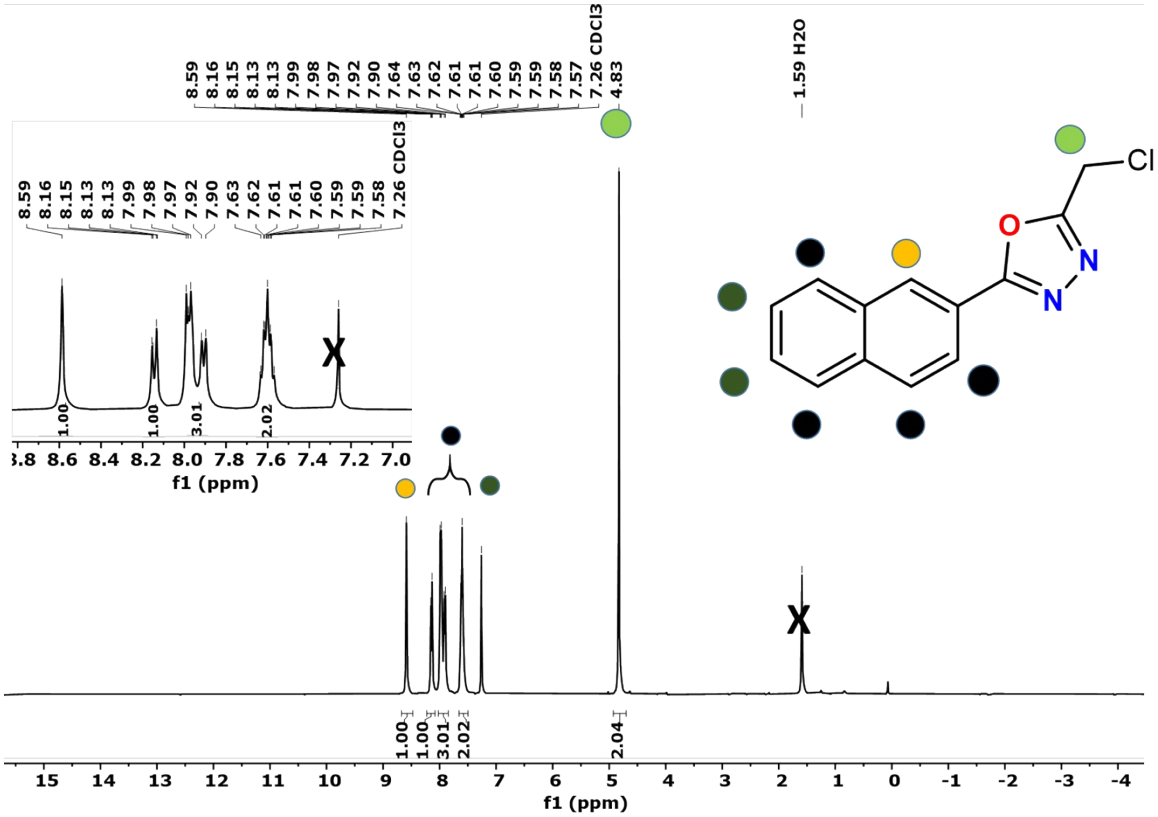

Figure S4: ^{1}H-NMR-spectra of 2-(Chloromethyl)-5-(naphthalen-2-yl)-1,3,4-oxadiazole (**IV**) in D^{6}- $CDCl_3$.

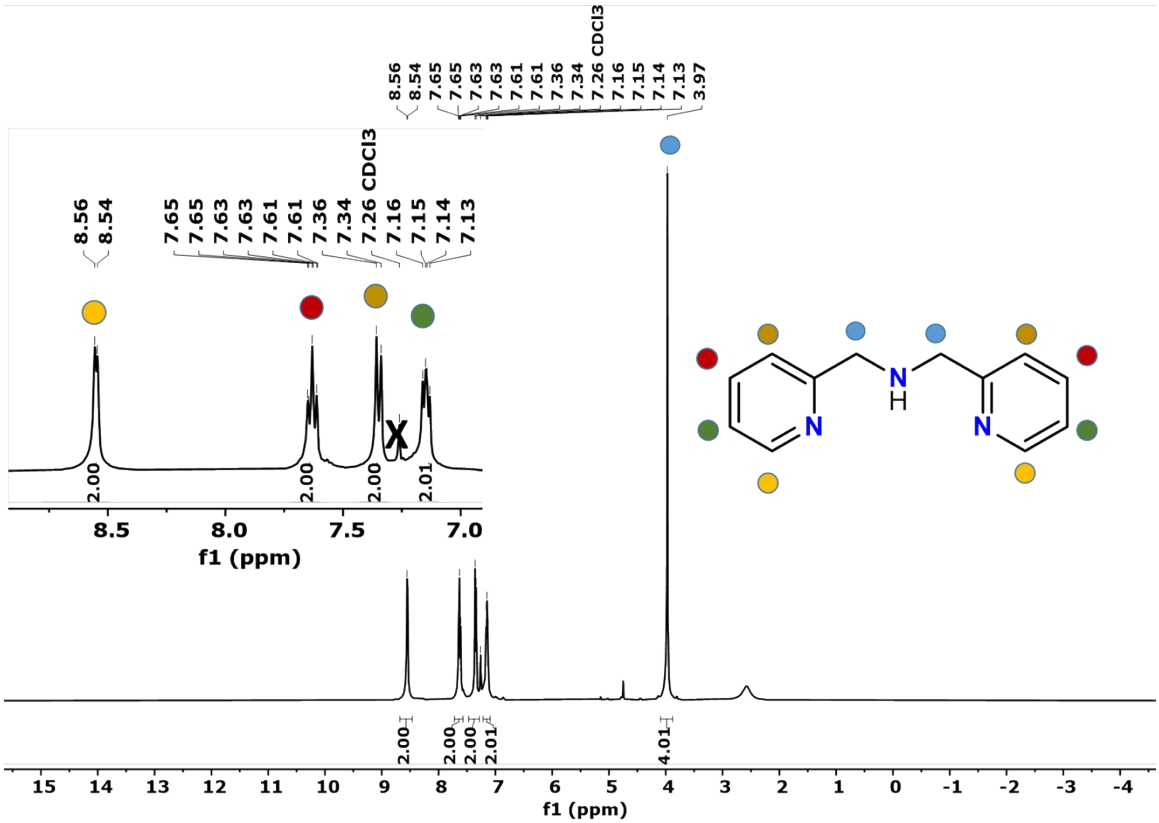

Figure S5: ^{1}H-NMR-spectra of Bis[(2-pyridyl)methyl]amine (**V**) in $CDCl_3$.

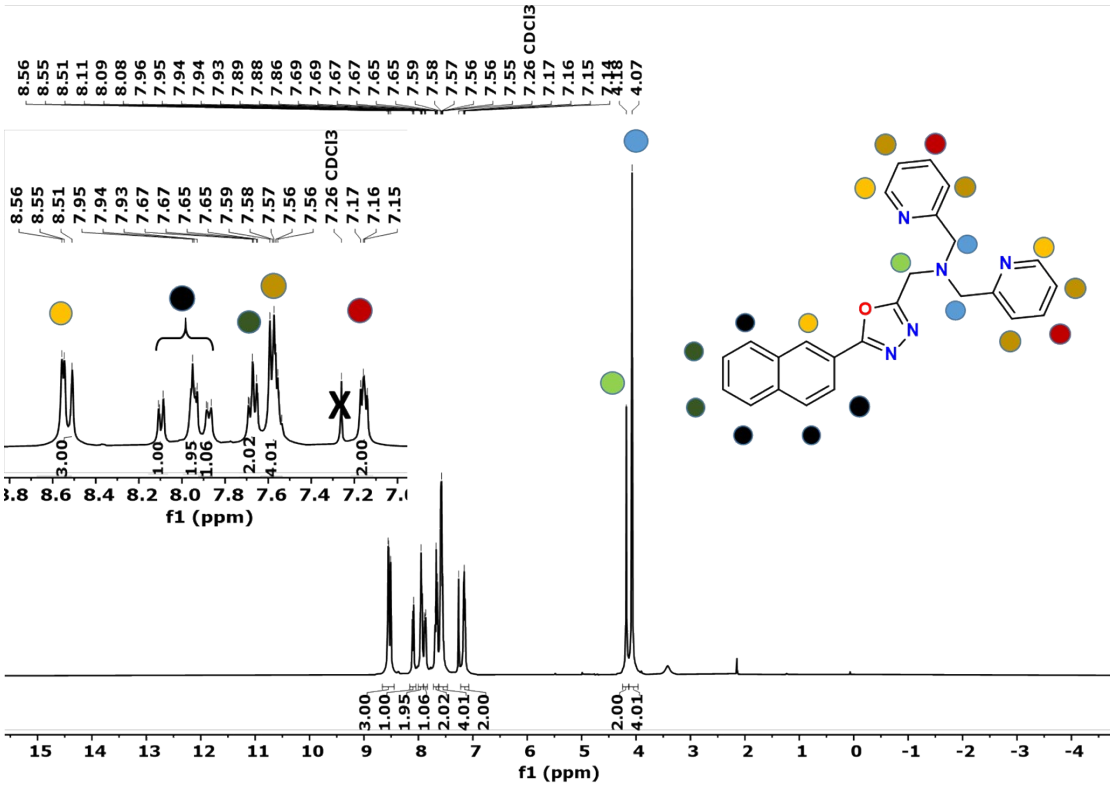

Figure S6: ^{1}H-NMR-spectra of 2-(Naphthalen-2-yl)-5-[N,N-bis(2-pyridylmethyl)aminomethyl]-1,3,4-oxadiazole (**L**$^{\text{Tetra-ODA}}$) in $CDCl_3$.

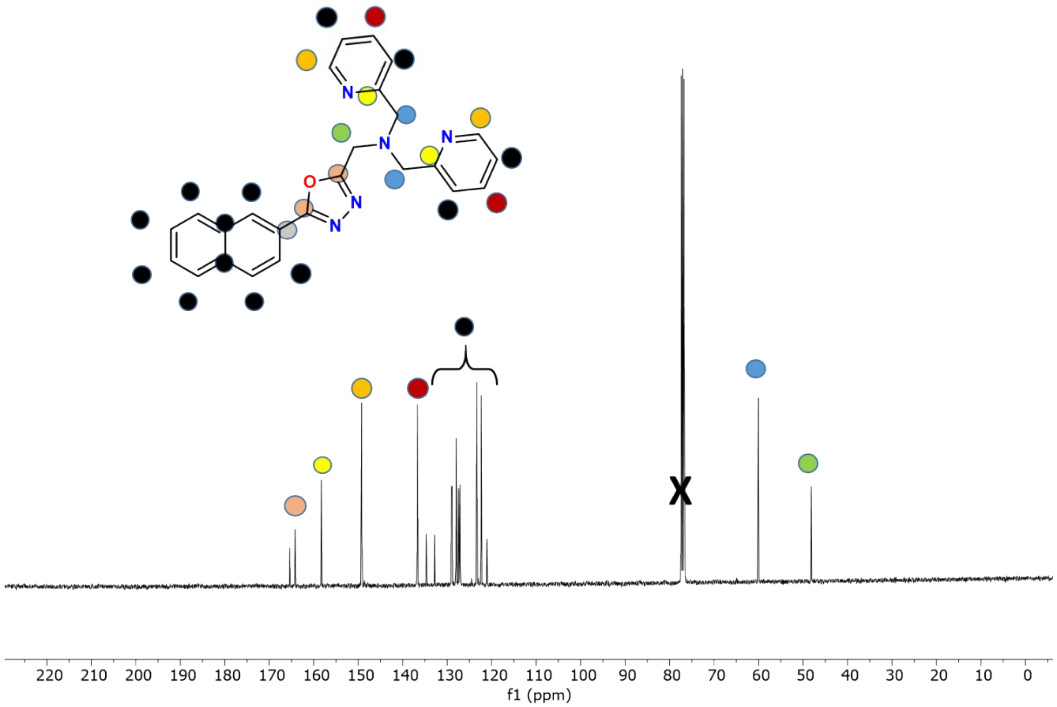

Figure S7: ^{13}C-NMR-spectra of 2-(Naphthalen-2-yl)-5-[N,N-bis(2-pyridylmethyl)aminomethyl]-1,3,4-oxadiazole (**L**$^{\text{Tetra-ODA}}$) in $CDCl_3$.

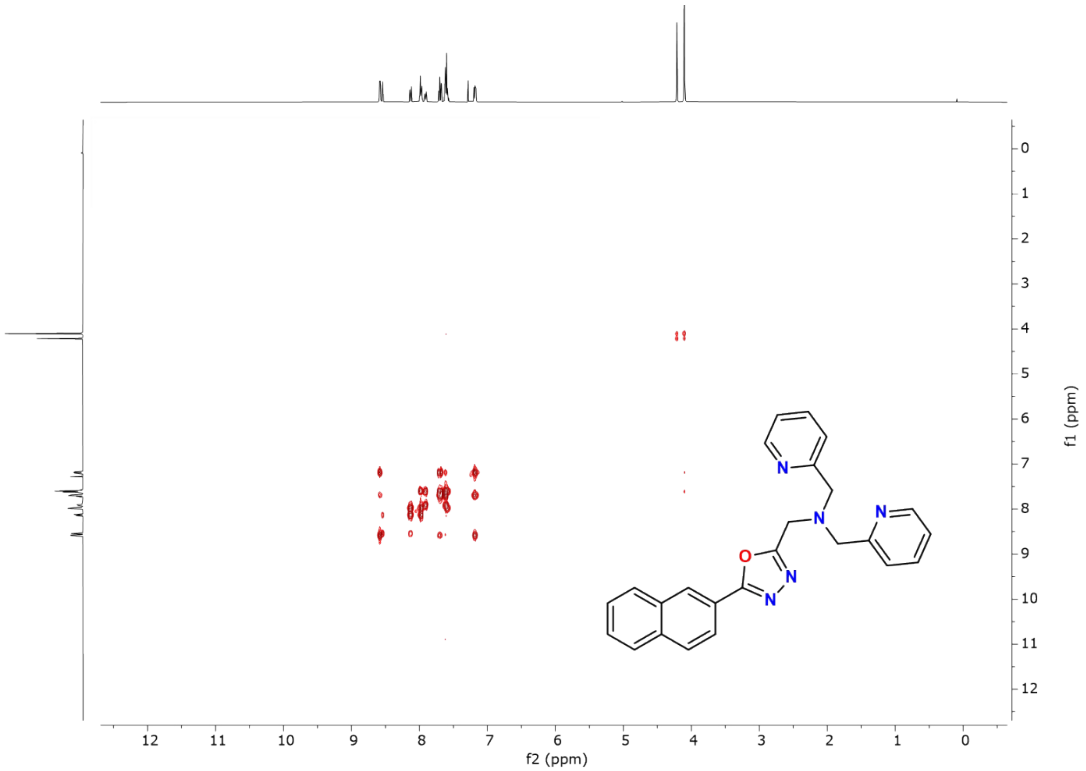

Figure S8: COSY-NMR-spectra of ($L^{Tetra\text{-}ODA}$) 2-(Naphthalen-2-yl)-5-[N,N-bis(2-pyridylmethyl)aminomethyl]-1,3,4-oxadiazole in $CDCl_3$.

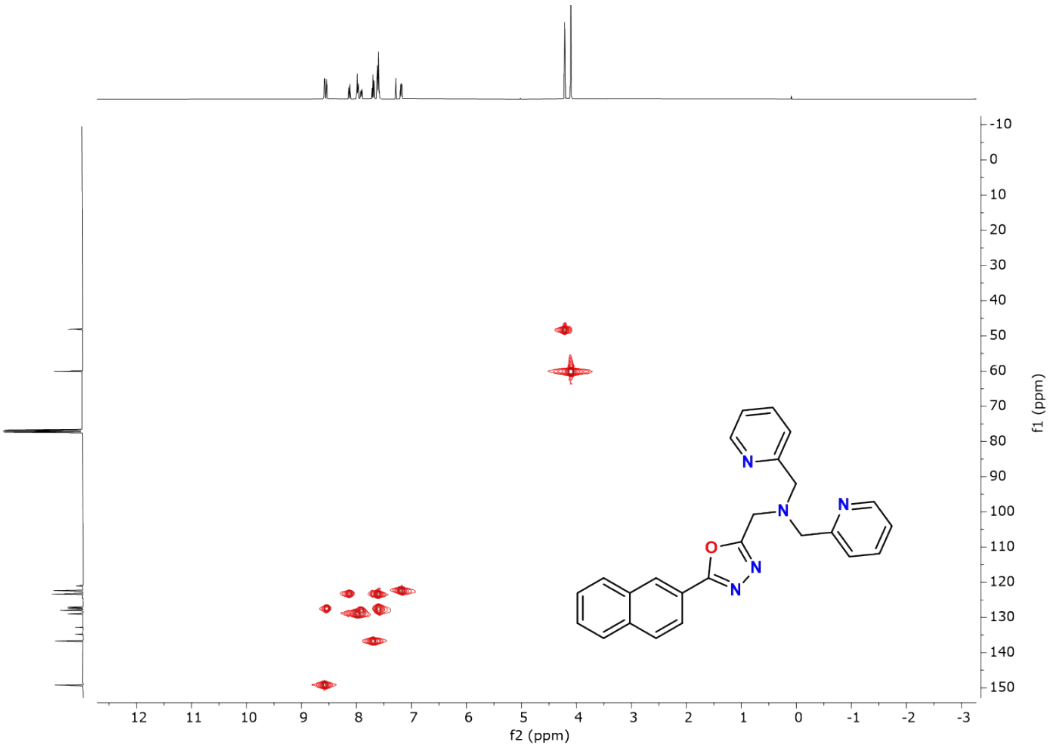

Figure S9: HSCQ-NMR-spectra of 2-(Naphthalen-2-yl)-5-[N,N-bis(2-pyridylmethyl)aminomethyl]-1,3,4-oxadiazole ($L^{Tetra\text{-}ODA}$) in $CDCl_3$.

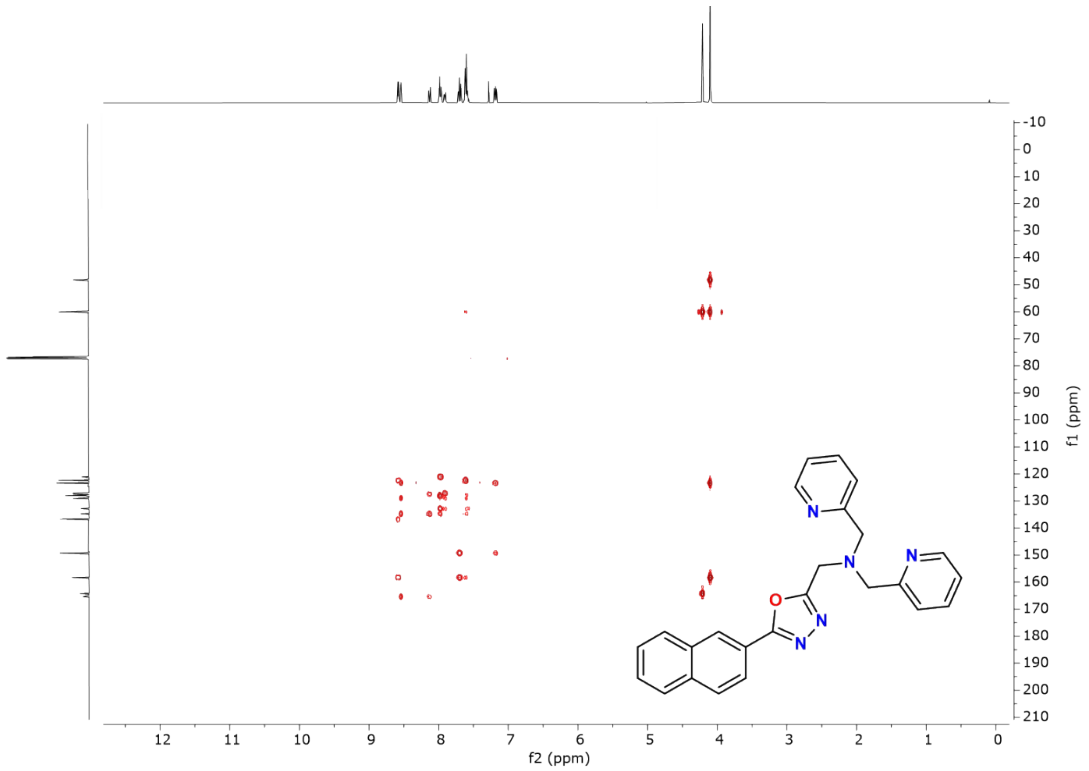

Figure S10: HMBC-NMR-spectra of 2-(Naphthalen-2-yl)-5-[N,N-bis(2-pyridylmethyl)aminomethyl]-1,3,4-oxadiazole (**L**$^{\text{Tetra-ODA}}$) in $CDCl_3$.

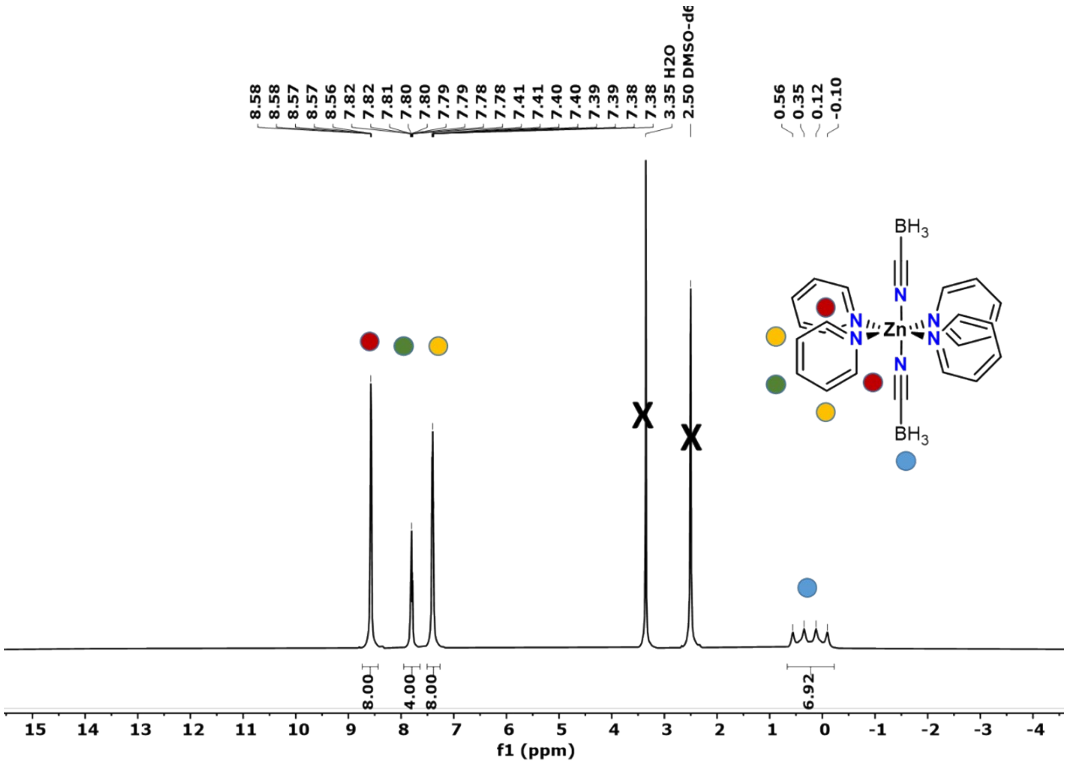

Figure S11: ^{1}H-NMR-spectra of $[Zn(py)_4(NCBH_3)_2]\cdot 0.5H_2O$ in D^{6}-DMSO.

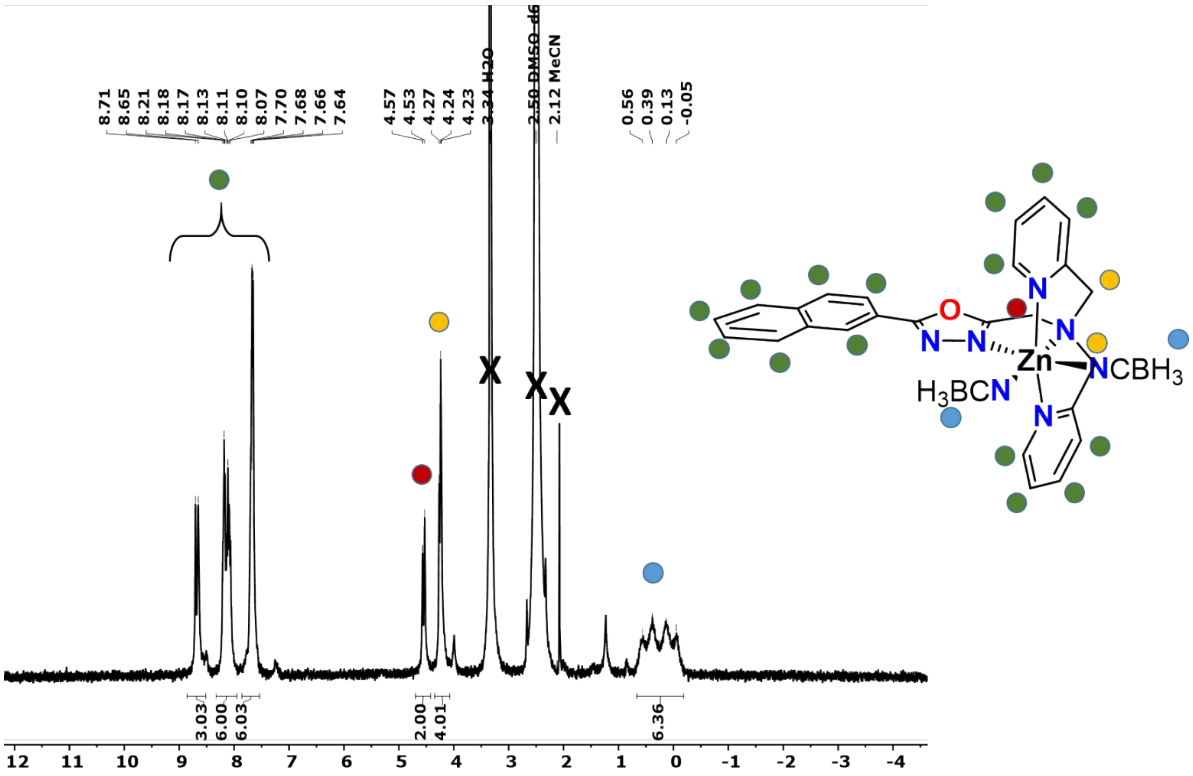

Figure S12: ^{1}H-NMR-spectra of [Zn(**L**$^{\textbf{Tetra-ODA}}$)(NCBH$_3$)$_2$]·0.5H$_2$O (**C2**) in D^{6}-DMSO.

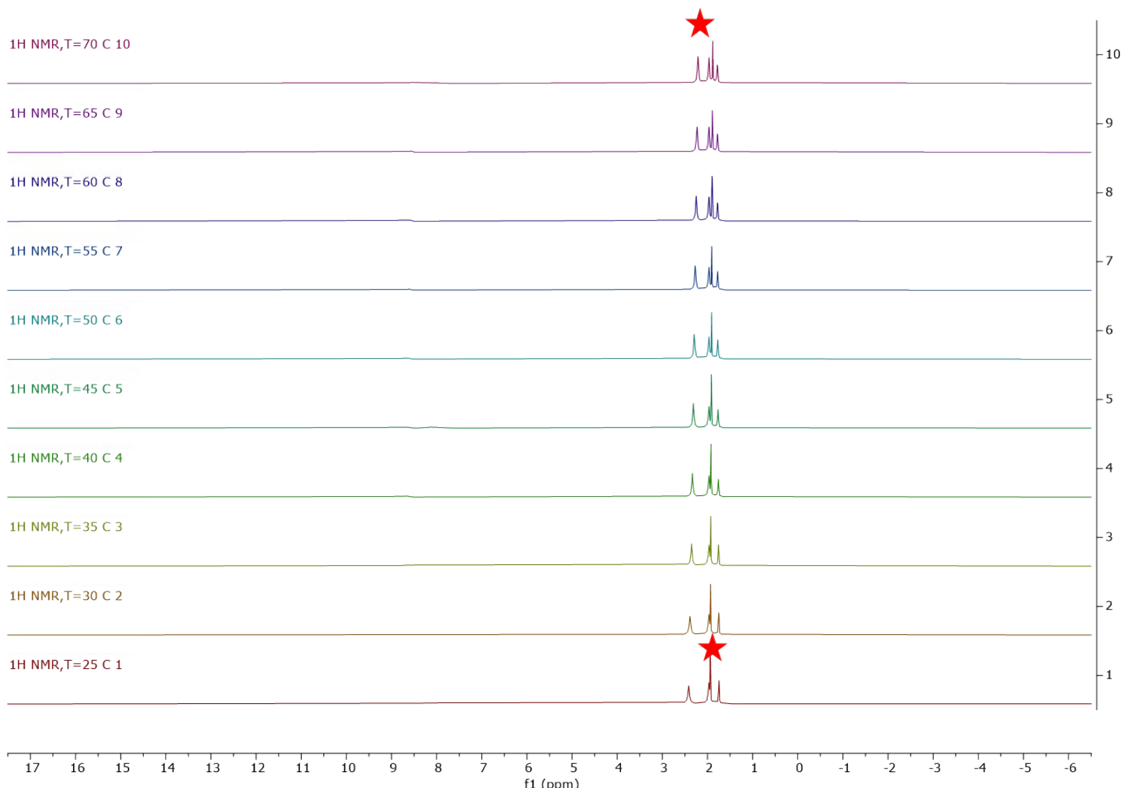

Figure S13: Temperature dependent Evans-measurement of [Fe(L$^{\text{Tetra-ODA}}$)(NCBH$_3$)$_2$]·1.5CH$_3$OH in D^{3}-MeCN.

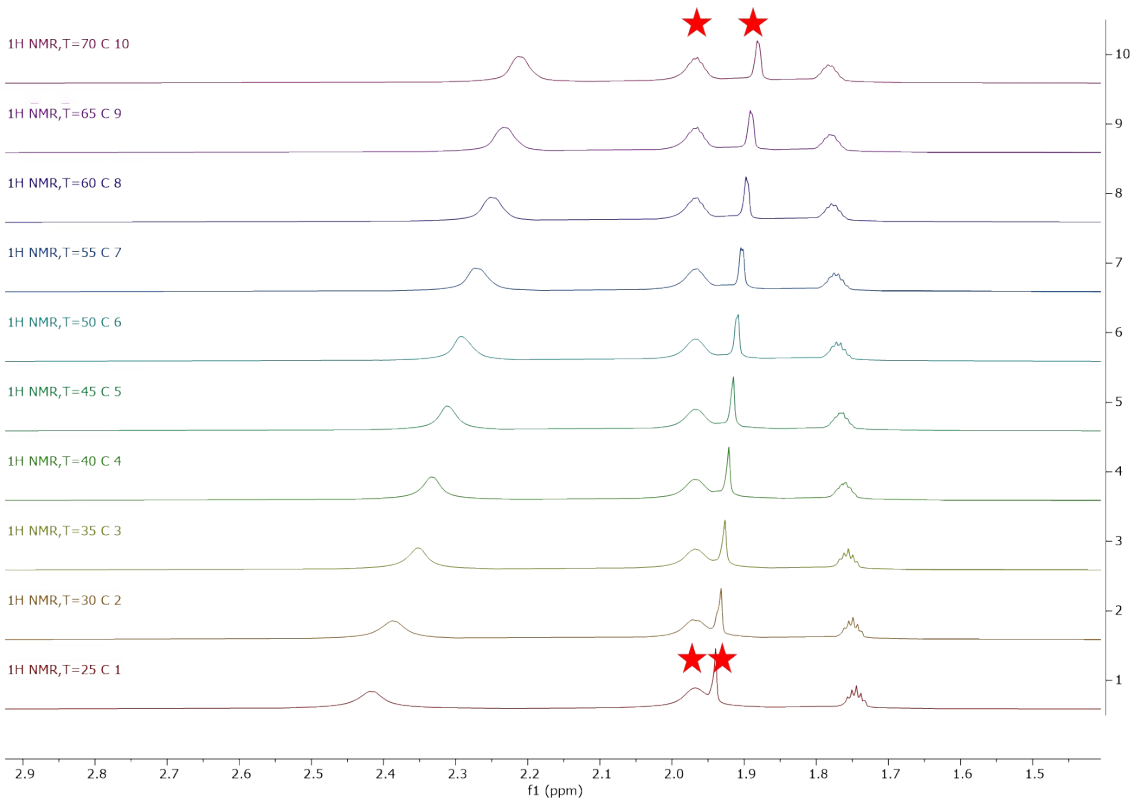

Figure S14: Temperature dependent Evans-measurement of [Fe(**L**$^{\textbf{Tetra-ODA}}$)$(NCBH_3)_2$] ·1.5CH_3OH in D^3-MeCN.

2. IR-spectra:

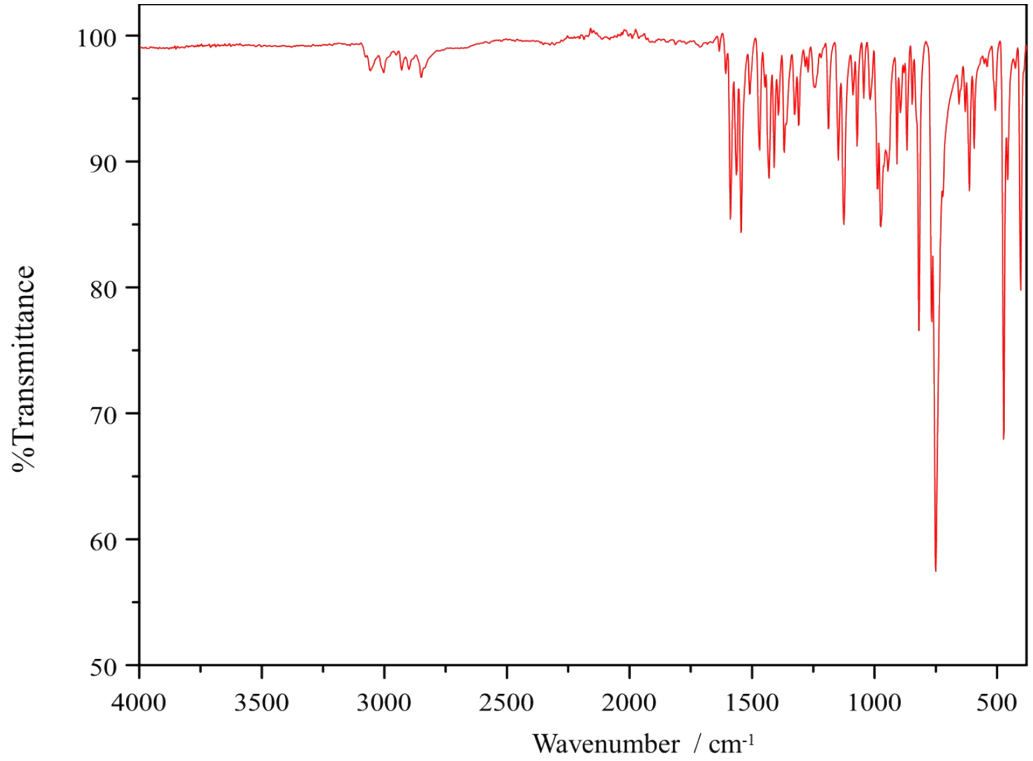

Figure S15: IR spectrum of 2-(Naphthalen-2-yl)-5-[N,N-bis(2-pyridylmethyl)aminomethyl]-1,3,4-oxadiazole ($\mathbf{L^{Tetra\text{-}ODA}}$).

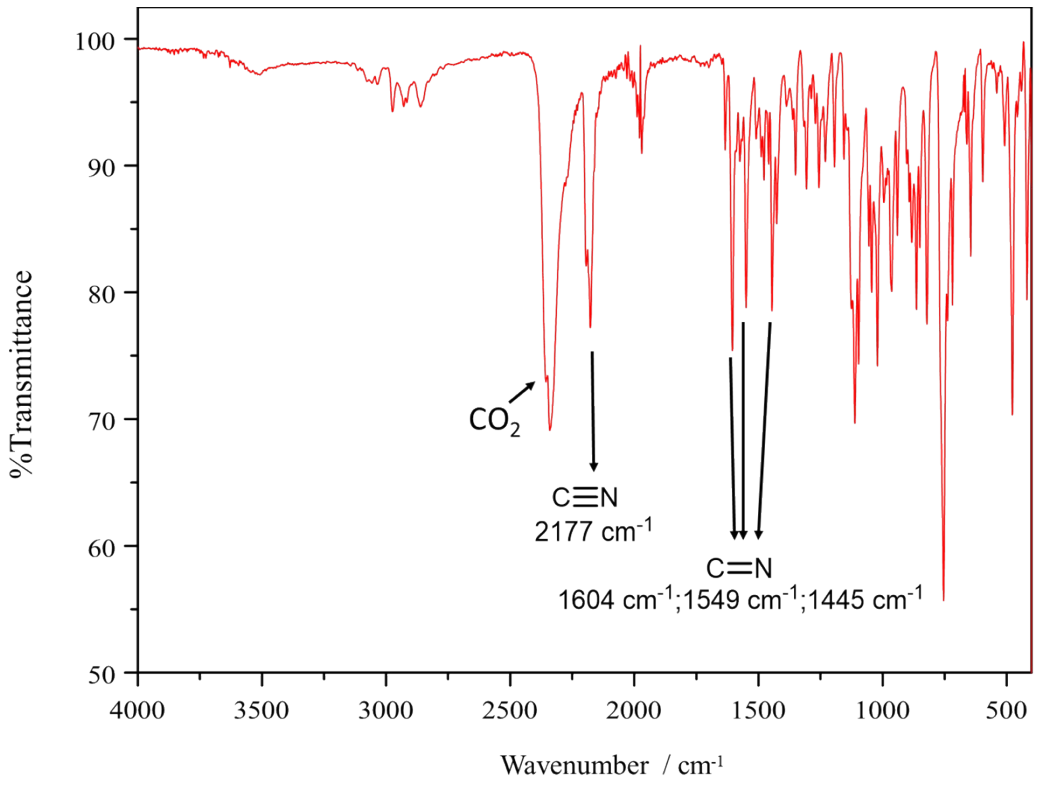

Figure S16: IR spectrum of $[Fe(L^{Tetra\text{-}ODA})(NCBH_3)_2]\cdot 1.5\ CH_3OH$ (**C1**)

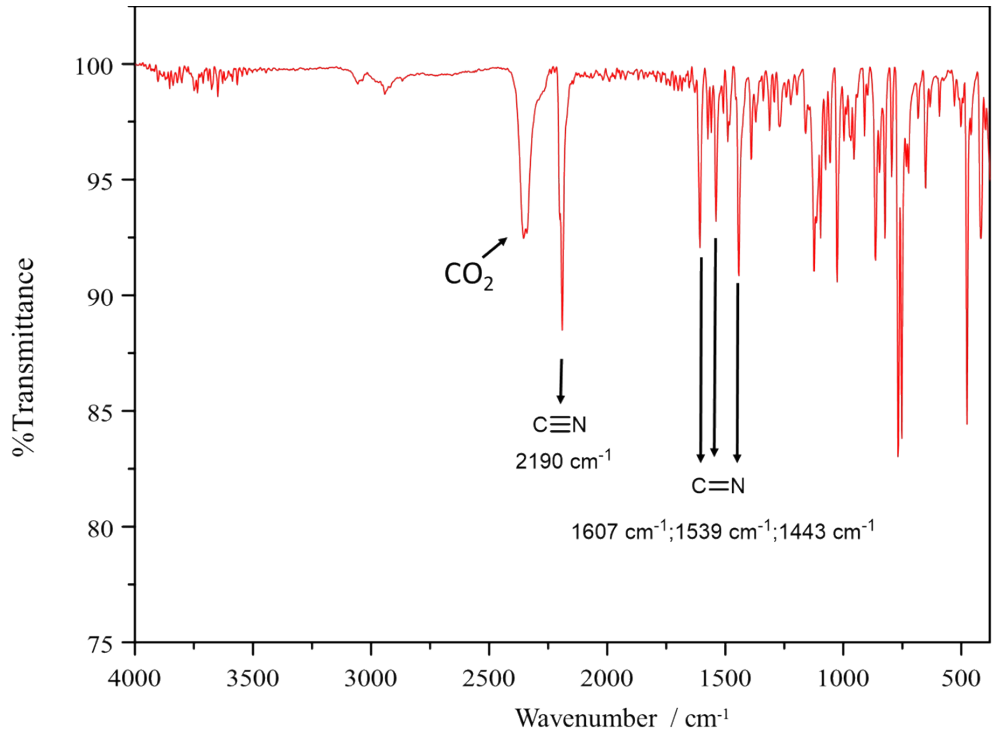

Figure S17: IR spectrum of $[Zn(L^{Tetra\text{-}ODA})(NCBH_3)_2]\cdot 0.5H_2O$ (**C2**).

3. Mass spectra:

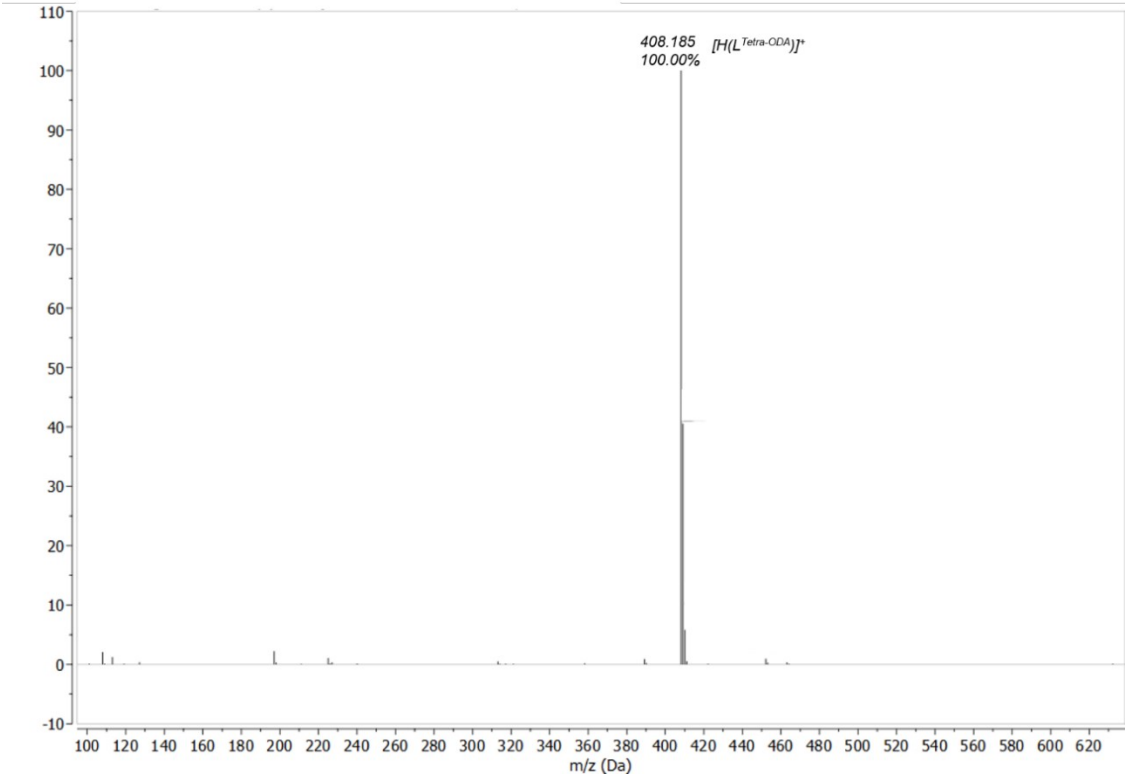

Figure S18: ESI mass spectrum of 2-(Naphthalen-2-yl)-5-[N,N-bis(2-pyridylmethyl)aminomethyl]-1,3,4-oxadiazole (**L$^{\text{Tetra-ODA}}$**).

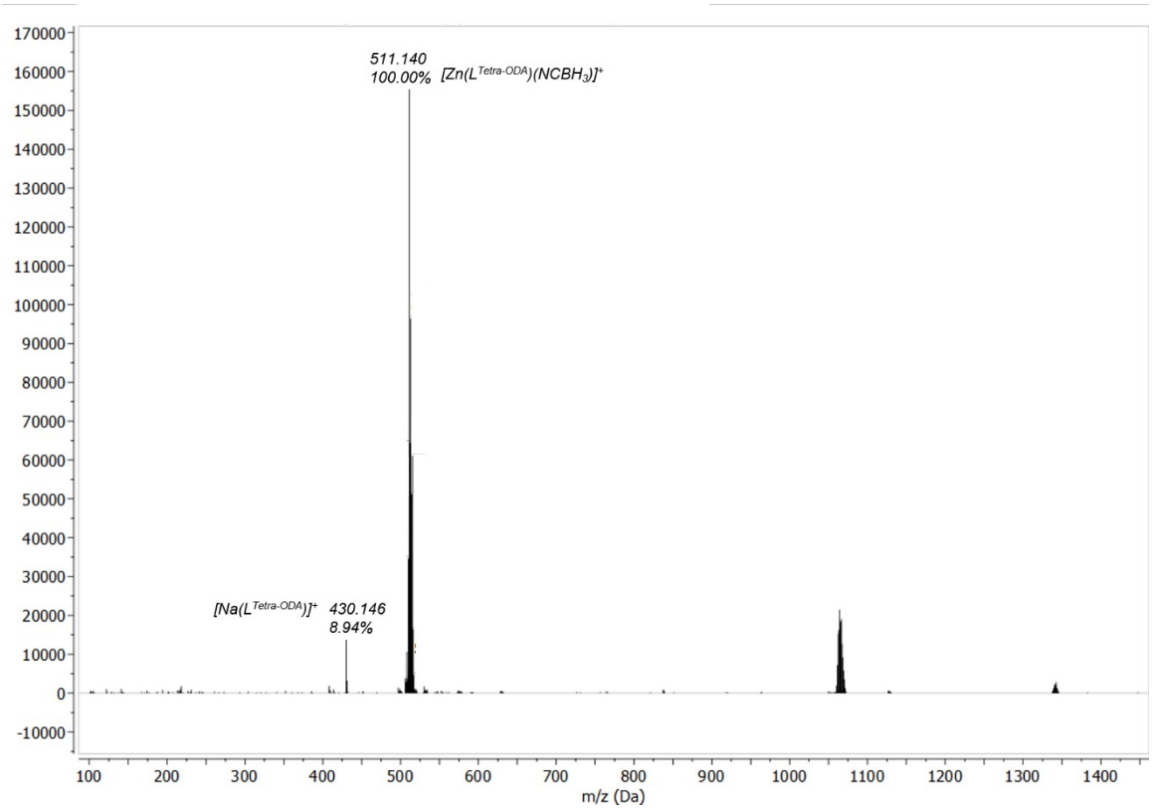

Figure S19: ESI mass spectrum of [Zn(L$^{\text{Tetra-ODA}}$)(NCBH$_3$)$_2$]·0.5H$_2$O .

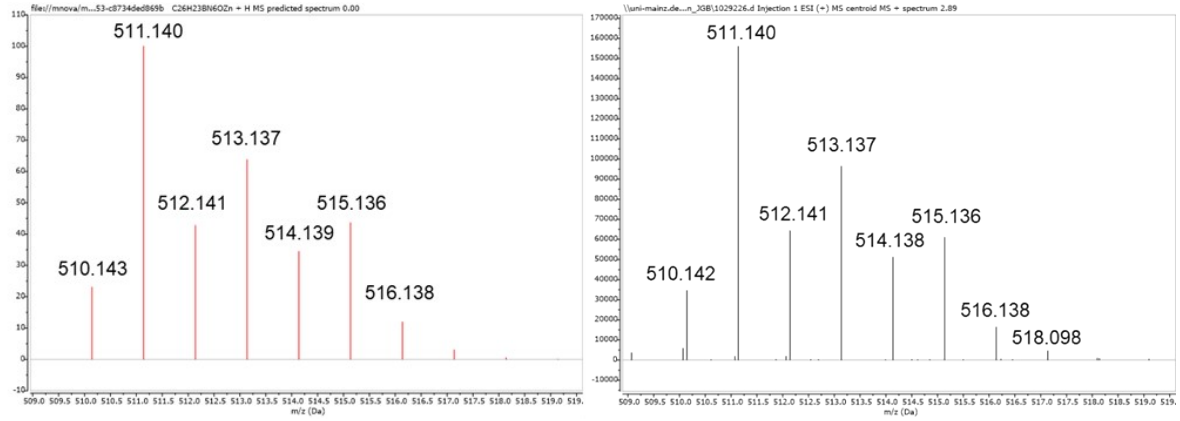

Figure S20: Isotopic pattern of ESI mass spectra of [Zn($L^{\mathbf{Tetra\text{-}ODA}}$)($NCBH_3$)$_2$]·0.5$H_2O$: *predicted (left) and measured (right)*.

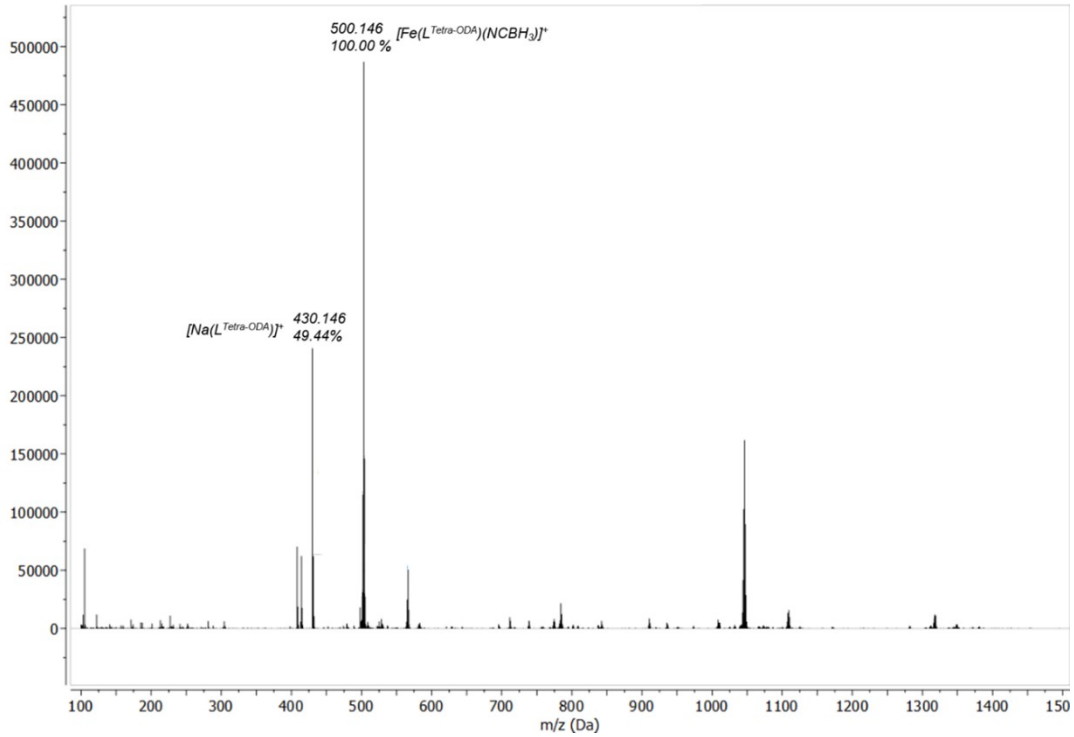

Figure S21: ESI mass spectrum of *[Fe($L^{\mathbf{Tetra\text{-}ODA}}$)($NCBH_3$)$_2$]*·1.5 CH_3OH (**C1**)

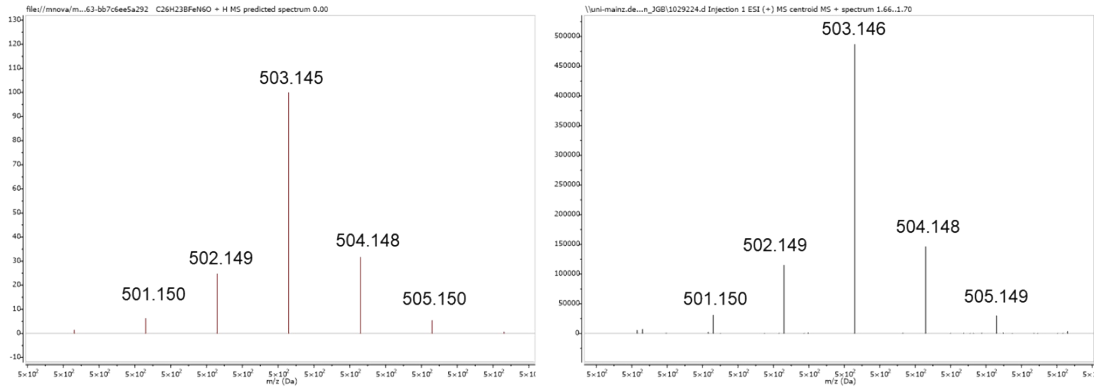

Figure S22: Isotopic pattern of ESI mass spectra of [Fe($L^{\mathbf{Tetra\text{-}ODA}}$)($NCBH_3$)$_2$]·1.5 CH_3OH (**C1**): *predicted (left) and measured (right).*

4. Crystal structures:

Table S1: Crystallographic Data of [Fe($L^{Tetra-ODA}$)($NCBH_3$)$_2$]·1.5 CH_3OH at 220 K and 120 K

Compound	**C1** (220 K)	**C1** (120 K)
Empirical formula	($C_{27}H_{27}B_2FeN_7O$) 1.5(CH_4O)	($C_{27}H_{27}B_2FeN_7O$) 1.5(CH_4O)
Formula weight / g mol^{-1}	591.09	591.09
Crystal size / mm	0.2 x 0.187 x 0.18	0.23 x 0.19 x 0.15
Crystal system	monoclinic	monoclinic
Space group	*C*2/*c*	*C*2/*c*
Unit cell dimensions		
a / Å	26.7229(7)	26.0632(7)
b / Å	10.9749(2)	10.5691(2)
c / Å	21.1290(6)	21.3067(6)
α / °	90	90
β / °	95.813(2)	96.182(2)
γ / °	90	90
Volume / Å	6164.9(3)	5835.1(3)
Z	8	8
$\rho_{calc.}$ / g cm^{-1}	1.266	1.346
μ / mm^{-1}	0.528	0.558
F(000)	2454	2472
Temperature / K	220	120
Diffractometer	STOE STADIVARI	STOE STADIVARI
Radiation	Mo-Kα	Mo-Kα
ϑ – range for data collection / °	1.938 < ϑ < 31.123	1.923 < ϑ < 30.771
Index ranges	-38 < h < 36	-36 < h < 37
	-15 < k < 15	-15 < k < 15
	-30 < l < 30	-30 < l < 30
Collected reflections	56550	51641
Independent reflections	58044	53070
Completeness	0.908	0.929
Max. and min. transmission	0.9893 and 0.4678	0.9090 and 0.2842
R_{int}	0.0364	0.0308
R_{sigma}	0.0318	0.0291
Data/ restraints/ parameters	9010 / 38 / 404	8470 / 31 / 403
Goodness-of-fit on F^2	0.977	1.078
Final R_1 [$I \geq 2\sigma(I)$]	0.0455	0.0444
Final wR_2 [$I \geq 2\sigma(I)$]	0.1354	0.1316
Final R_1 [*alldata*]	0.0638	0.0573
Final wR_2 [*alldata*]	0.1438	0.1369

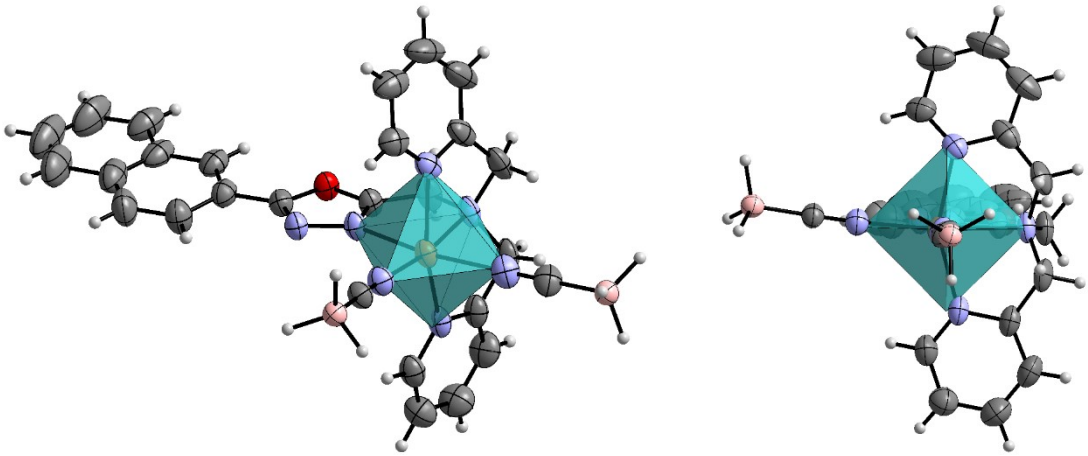

Figure S23: Molecular structure of *[Fe(**L**$^{Tetra\text{-}ODA}$)(NCBH$_3$)$_2$]*·1.5 CH$_3$OH and it is ideal coordination octahedron with front view (left) and view along the Fe-N5 axis (right), calculated with SHAPE. Colour scheme: dark grey – C, grey – H, violet – N, red – O, bright orange – Se, orange – Fe. ORTEP representation with atomic displacement parameters set to 50 % probability.

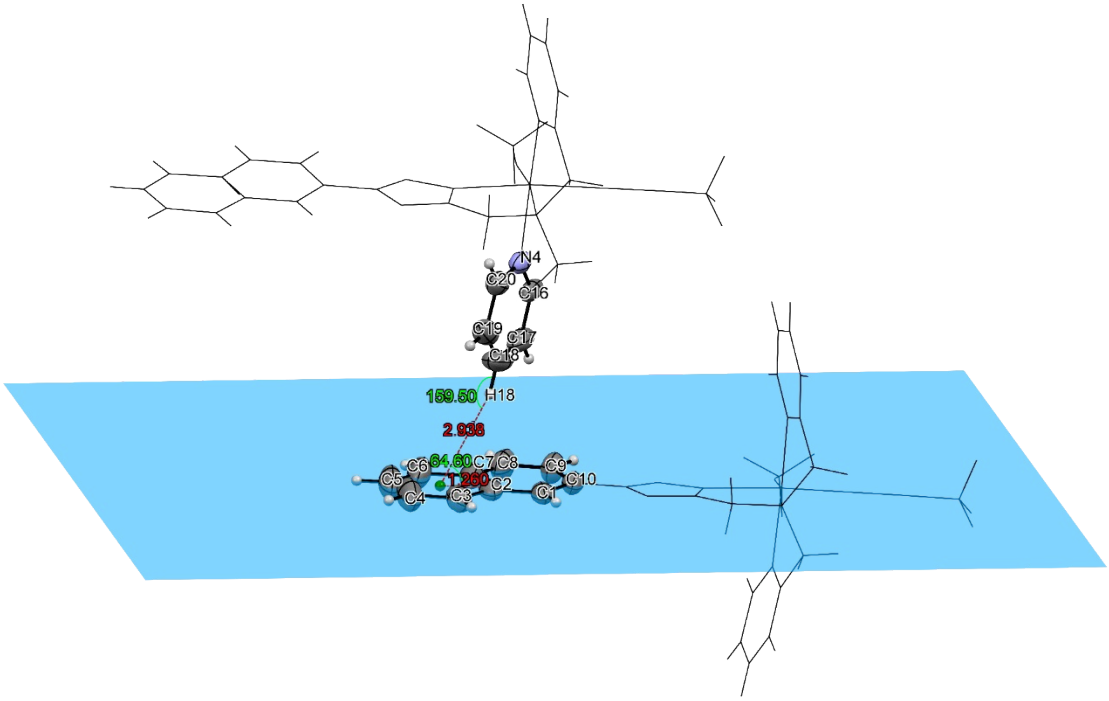

Figure S24: C-H ··· π interaction in *[Fe(**L**$^{Tetra\text{-}ODA}$)(NCBH$_3$)$_2$]*·1.5 CH$_3$OH (240 K). Least-squares plane A is defined by C2, C3, C4, C5, C6 and C7. Interacting C-H fragment is labeled as C18-H18. Green point – center of the aromatic ring in A. Purple point – orthogonal intersection of H18 onto plane A. *Offset* r = 1.26 Å, *interaction distance* d_{QH} = 2.94 Å, α = 159.5 ° and β = 64.6 °. ORTEP representation with atomic displacement parameters set to 50 % probability.

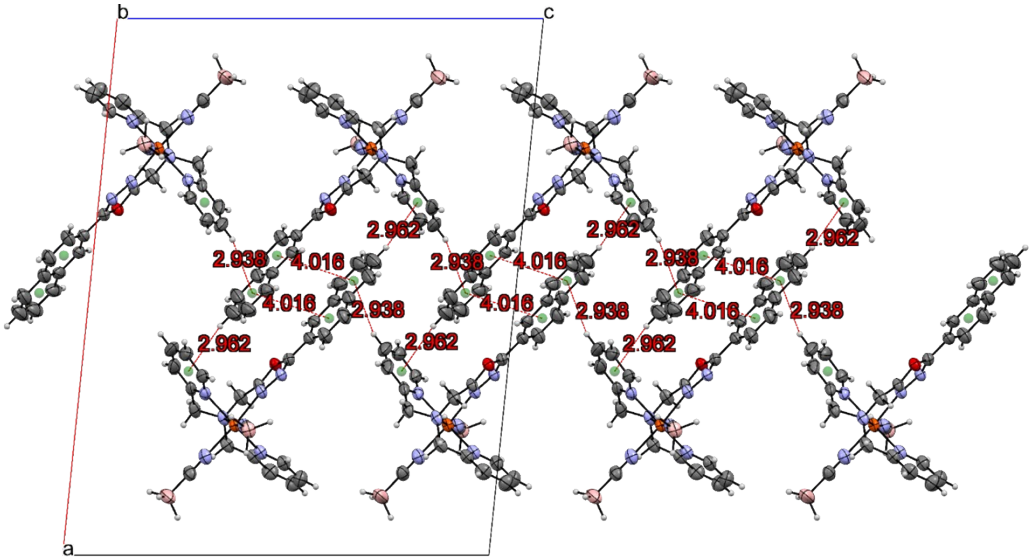

Figure S25: One-dimensional network of "complex dimers" in *[Fe(**L**$^{Tetra\text{-}ODA}$)(NCBH$_3$)$_2$]*·1.5 CH$_3$OH. Red dashed lines represent intermolecular distances. Colour scheme: pink – B, dark grey – C, grey – H, violet – N, red – O, orange – Fe. ORTEP representation with atomic displacement parameters set to 50 % probability.

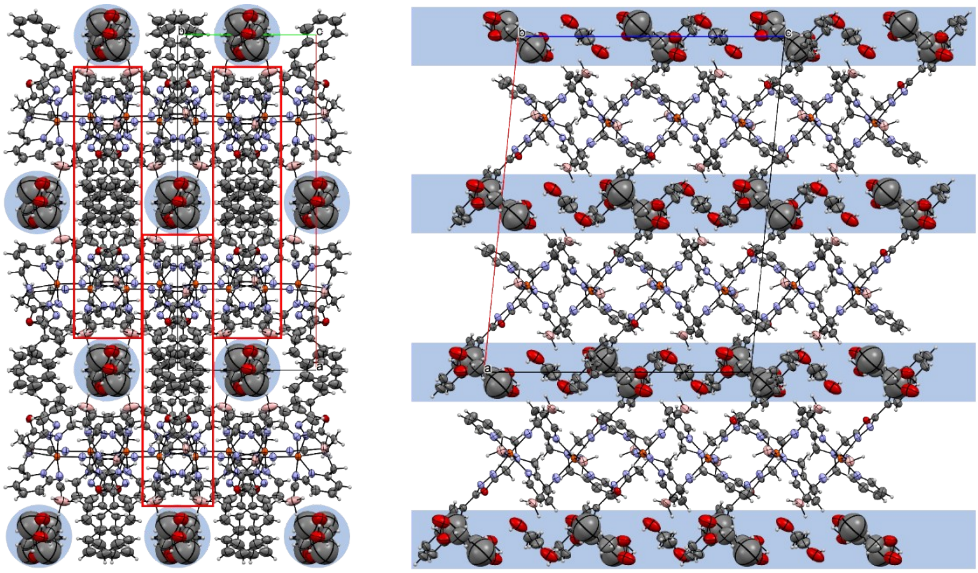

Figure S26: Packing of [Fe(**L**$^{Tetra\text{-}ODA}$)(NCBH$_3$)$_2$]·1.5 CH$_3$OH with view along the c-axis (left) and view along the b-axis (right). Red rectangles mark the one-dimensional chains of complex molecules along the c-axis. Blue areas illustrate the channel of solvent molecules. Colour scheme: pink – B, dark grey – C, grey – H, violet – N, red – O, orange – Fe. ORTEP representation with atomic displacement parameters set to 50 % probability.

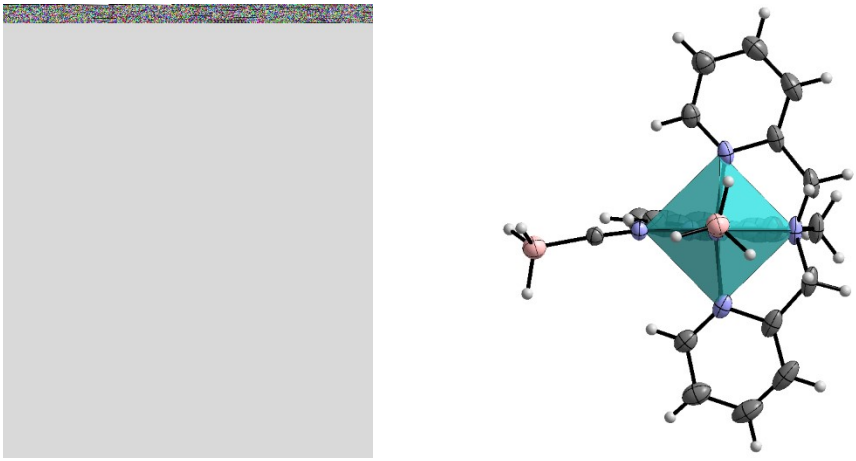

Figure S27: Molecular structure of [Fe($\mathbf{L}^{\mathbf{Tetra\text{-}ODA}}$)$(NCBH_3)_2$]·1.5 CH_3OH and its ideal coordination octahedron with view along the Fe-N5 axis at 220 K (left) and 120 K (right), calculated with SHAPE. Colour scheme: pink – B, dark grey – C, grey – H, violet – N, red – O, orange– Fe. ORTEP representation with atomic displacement parameters set to 50 % probability.

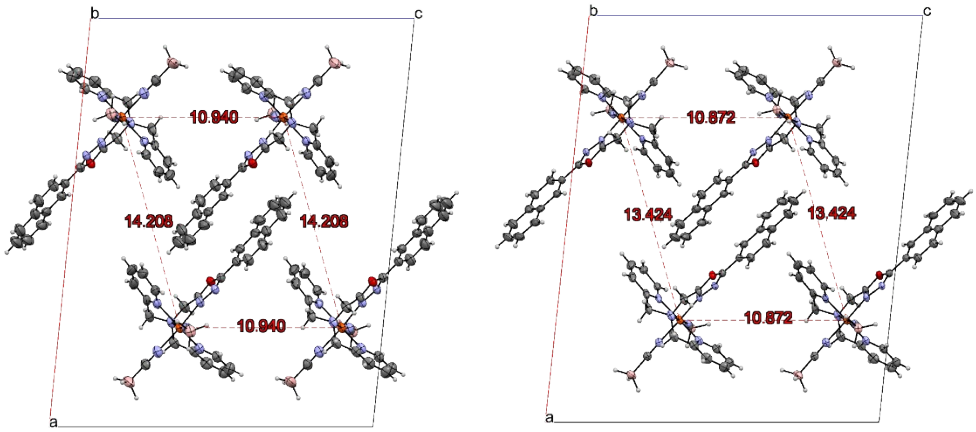

Figure S28 One-dimensional network of "complex dimers" in [Fe($\mathbf{L}^{\mathbf{Tetra\text{-}ODA}}$)$(NCBH_3)_2$]·1.5 CH_3OH at 220 K (left) and 120 K (right). Unit cell changes are remarkably more pronounced along the a-axis, which corresponds to the interdimer short contacts. Red dashed lines represent intermolecular distances between iron(II) centers. Colour scheme: pink – B, dark grey – C, grey – H, violet – N, red – O, orange– Fe. ORTEP representation with atomic displacement parameters set to 50 % probability.

5. UV-Vis-Spectra:

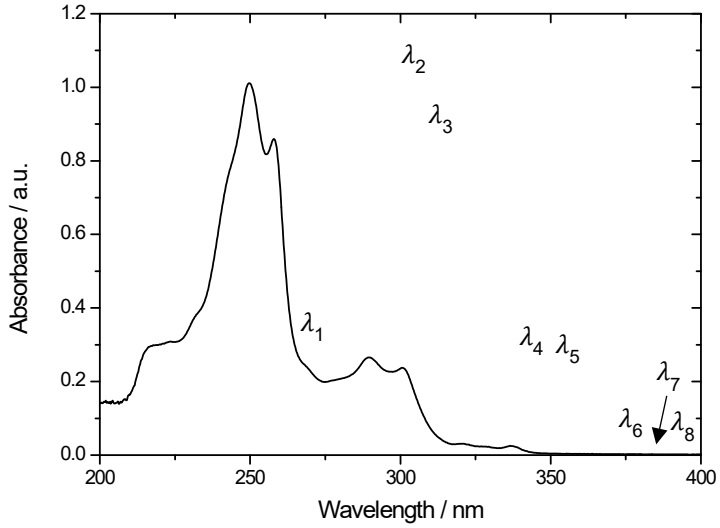

Figure S29: UV-Vis spectrum of $\mathbf{L^{Tetra\text{-}ODA}}$ in n-butyronitril (c = 0.03 mmol/l).

Table S2: Summary of the present absorption maxima λ_i in the UV/Vis spectrum of $\boldsymbol{L^{Tetra\text{-}ODA}}$ in n-butyronitril with corresponding molar extinction coefficients (ε) in $M^{-1}cm^{-1}$.

	λ_1	λ_2	λ_3	λ_4	λ_5	λ_6	λ_7	λ_8
λ_{abs} / nm	216	249	258	289	300	320	328	337
ε / $M^{-1}cm^{-1}$	15084	79001	67250	13506	11902	1068	775	850

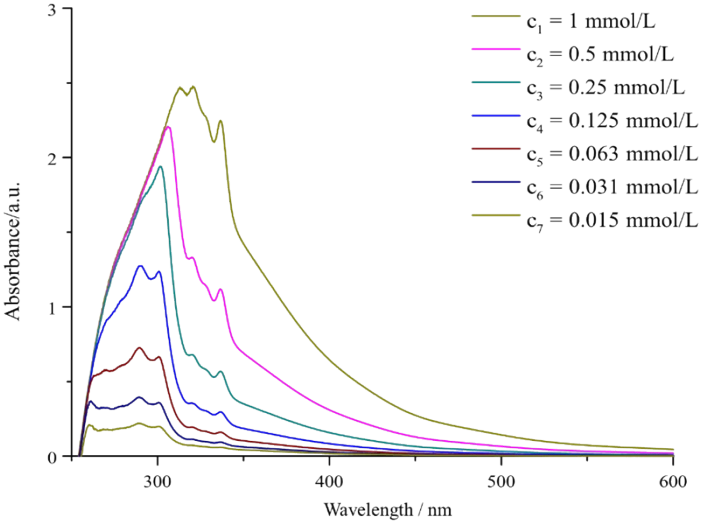

Figure 30: UV/Vis spectra of [Fe($\mathbf{L^{Tetra\text{-}ODA}}$)$(NCBH_3)_2$]·1.5 CH_3OH in n-butyronitrile for different concentrations. From measurement to measurement, the concentration was halved by diluting the solution. There is no absorption observable between 600-1000 nm.

Table S3: Summary of the present absorption maxima λ_i in the UV/Vis spectra of [Fe($\mathbf{L^{Tetra\text{-}ODA}}$)$(NCBH_3)_2$]·1.5 CH_3OH in n-butyronitrile with corresponding molar extinction coefficients ε in $M^{-1}cm^{-1}$.

	λ_1	λ_2	λ_3	λ_4	λ_5	λ_6
λ_{abs} / nm	258	289	301	320	328	337
ε / $M^{-1}cm^{-1}$	2657	2729	3192	12488	13588	12890

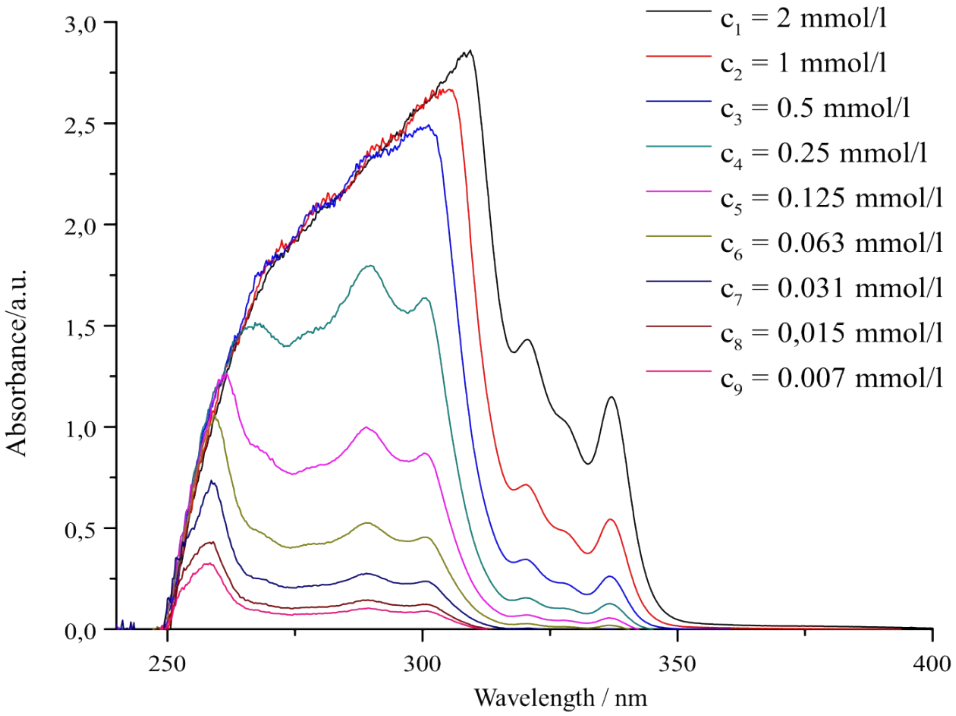

Figure S31: UV/Vis spectra of [Zn($\mathbf{L^{Tetra\text{-}ODA}}$)$(NCBH_3)_2$]·0.5$H_2O$ in n-butyronitrile for different concentrations. From measurement to measurement, the concentration was halved by diluting the solution. There is no absorption observable between 400-1000 nm.

6. Photoluminescence spectroscopy

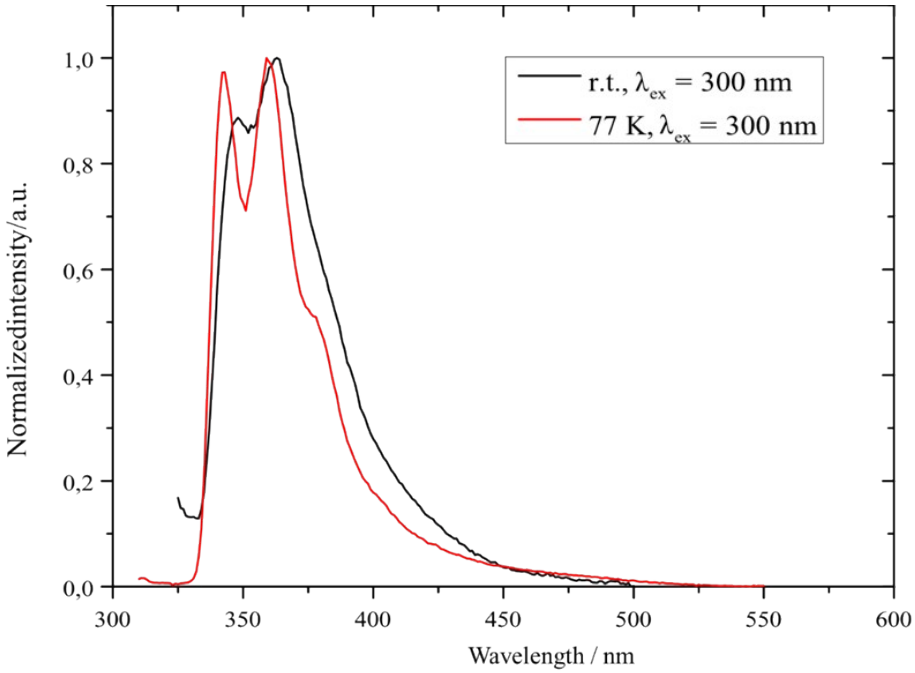

Figure S32: PL-spectra of [Fe($\mathbf{L}^{\mathbf{Tetra\text{-}ODA}}$)$(NCBH_3)_2$]·1.5 CH_3OH in solid state. Samples were excited with λ_{ex} = 300 nm. Measurements were done at 77 K (red solid lines) and at room temperature (black solid lines).

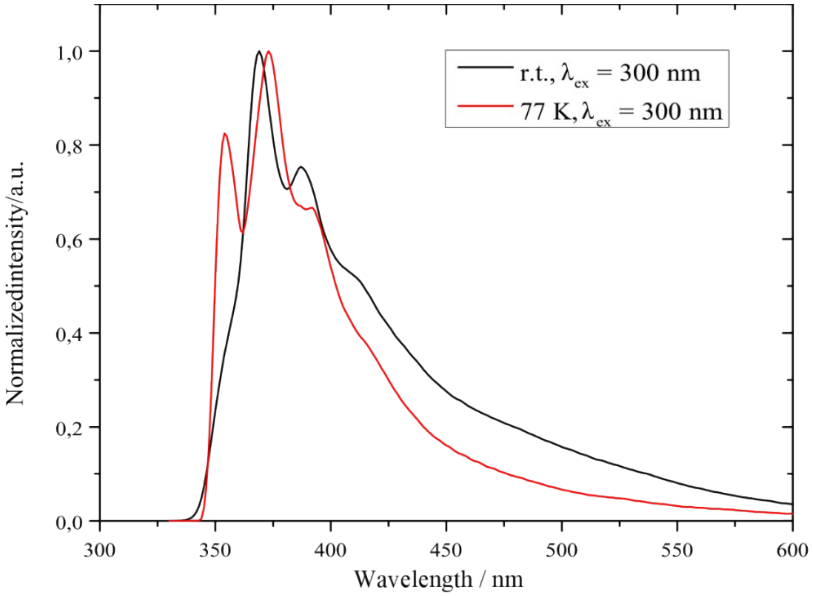

Figure S33: PL-spectra of [Zn($\mathbf{L}^{\mathbf{Tetra\text{-}ODA}}$)$(NCBH_3)_2$]·0.5$H_2O$ in solid state. Samples were excited with λ_{ex} = 300 nm. Measurements were done at 77 K (red solid lines) and at room temperature (black solid lines).

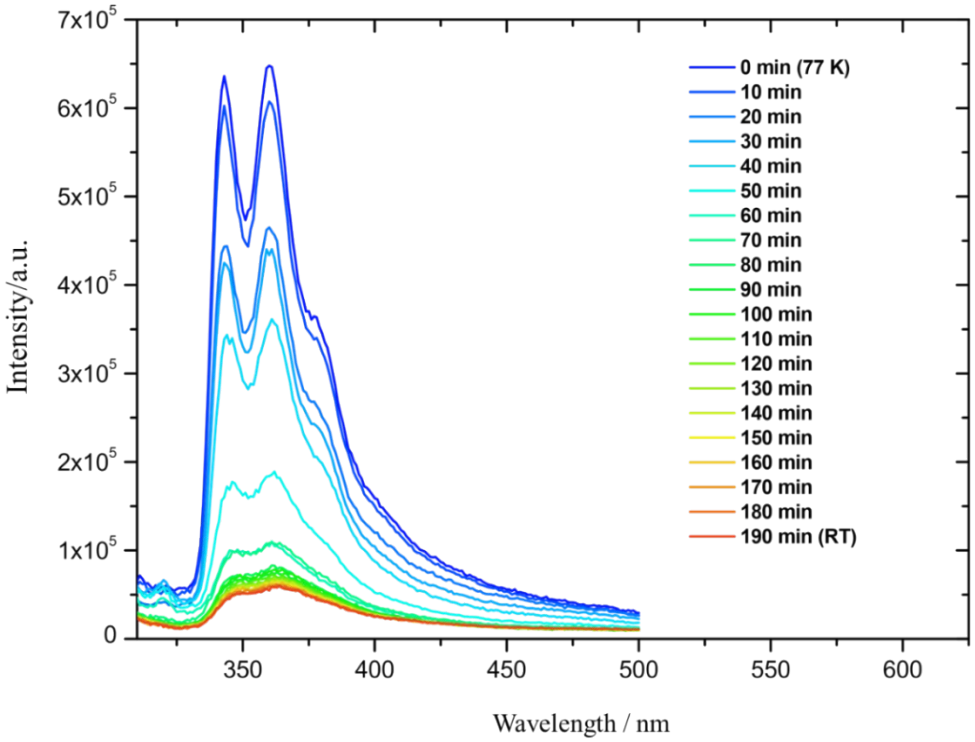

Figure S34: Emission spectra of [Fe(**L**$^{\text{Tetra-ODA}}$)$(NCBH_3)_2$]·1.5 CH_3OH between 310 nm and 500 nm for a series of time related measurements. During the measured 190 min, liquid nitrogen was allowed to evaporate, which results in a heating of the sample.

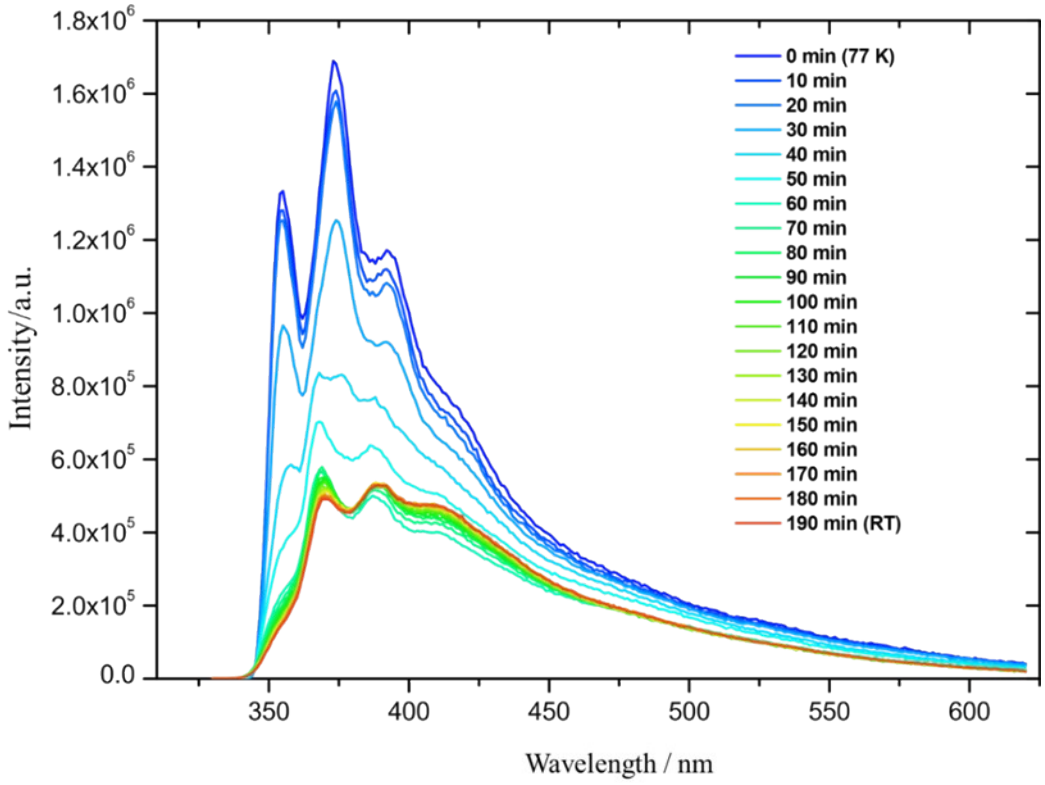

Figure S35: Emission spectra of [Zn(**L**$^{\text{Tetra-ODA}}$)$(NCBH_3)_2$]·0.5H_2O between 310 nm and 625 nm for a series of time related measurements. During the measured 190 min, liquid nitrogen was allowed to evaporate, which results in a heating of the sample.

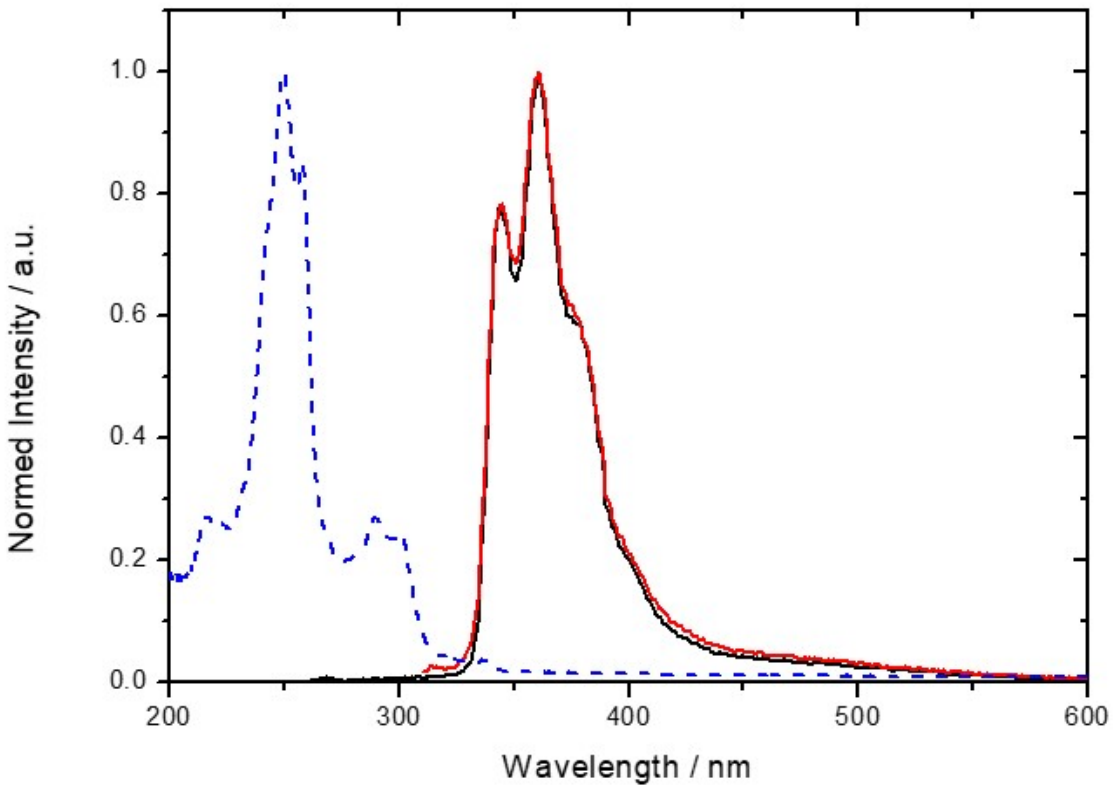

Figure S36: Combined intensity versus wavelength plot of absorption (blue dashed line) and emission spectra with excitation wavelengths of $\lambda_{ex,1}$ = 249 nm (black solid line) and $\lambda_{ex,2}$ = 289 nm (red solid line) of **L**$^{\textbf{Tetra-ODA}}$ in n-butyronitrile.

6. Magnetic Data:

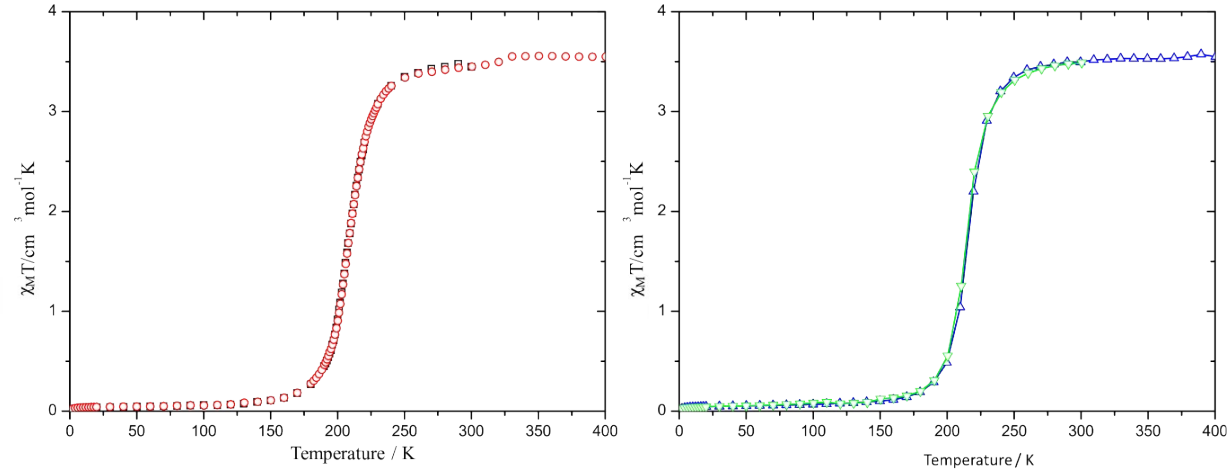

Figure S37: Temperature dependent magnetic behavior of single crystals of [Fe(**L**$^{\textbf{Tetra-ODA}}$)$(NCBH_3)_2$]·1.5 CH_3OH in the form of $\chi_M T$ *vs*. *T* plots. Left: Measurement between 300-2 K (black open squares) and 2-400 K (red open circles). Right: Subsequent measurement between 400-2 K (blue open triangles) and 2-300 K (green open triangles).

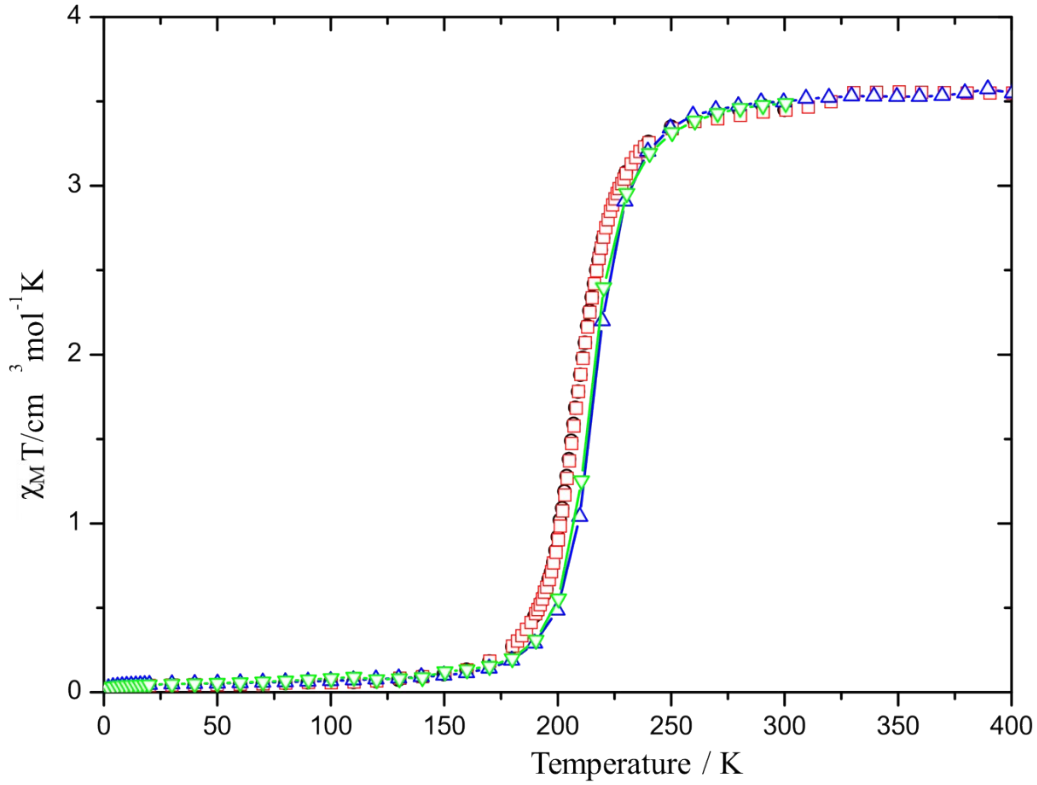

Figure S38: Temperature dependent magnetic behavior of single crystals of *[Fe(**L**$^{Tetra-ODA}$)(NCBH$_3$)$_2$]*·1.5 CH_3OH after five days under air in the form of the resulting $\chi_M T$ *vs*. *T* plot. Magnetic susceptibility was determined between 300-100 K (black open circles), 100-300 K (red open squares), 300-100 K (blue open squares) and 100-300 K (green open triangles).

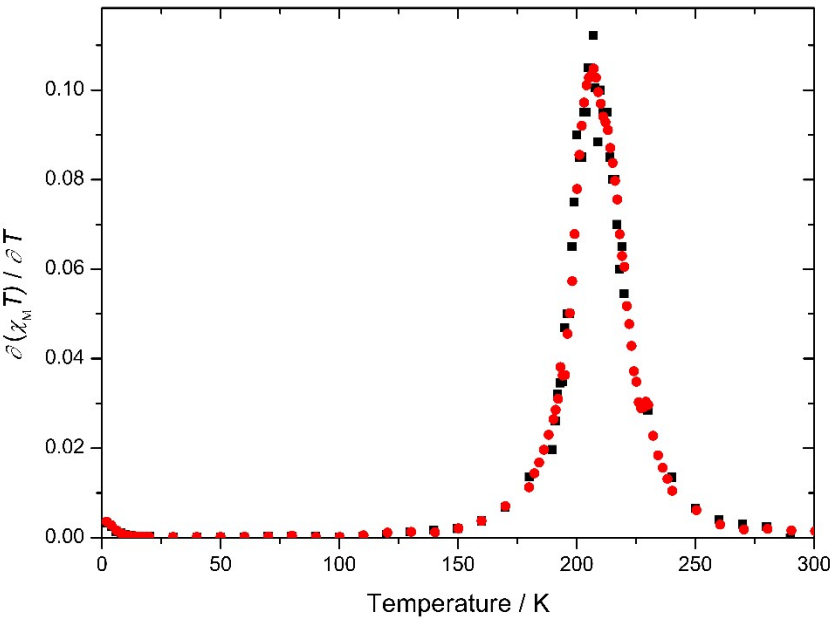

Figure S39: First derivative of $\chi_M T$ with respect to *T* for *[Fe(**L**$^{Tetra-ODA}$)(NCBH$_3$)$_2$]* ·1.5 CH_3OH. Susceptibility was measured from 300 K to 2 K (black open squares) and subsequently from 2 K to 400 K (red open circles).

The variable temperature Evans NMR data was measured in CD_3CN at a concentration of 5.06 X 10^{-3} M, from 298 to 343 K (at 5 K intervals) in heating mode *[Fe(**L**$^{Tetra\text{-}ODA}$)$(NCBH_3)_2]\cdot H_2O$.* Once the temperature is reached the sample is stabilized at that temperature for two minutes at each step before measuring. The methodology to calculate $\chi_M T$ from Evans ^1H NMR method data at a range of temperatures has been previously described.[1-2]

The modelling of each dataset as a gradual and complete SCO, using the regular solution model, equation (1) below,[3-4] resulted in good fits with R^2=0.98. For each data set, the fit gives ΔH and ΔS, the thermodynamic enthalpy and entropy values associated with the spin crossover. From these two values the $T_{1/2}$ value can be calculated, simply by dividing ΔH/ΔS, as ΔG = 0 at $T_{1/2}$ (and ΔG = ΔH – TΔS). The derived parameters are reported in Tables S1 and S2.

$\chi_M T(T) = \chi_M T(max) / 1 + e^{((-\Delta H/RT) + (\Delta S/R))}$ (S1)[3-4]

Where:

$\chi_M T(T)$ is $\chi_M T$ measured at temperature T,

$\chi_M T(max)$ is the maximum $\chi_M T$ value, which herein was set to 4.0 emu K mol^{-1} as this value falls within the expected literature range for iron(II) complexes.[5-6]

R is the ideal gas constant (8.314 J mol^{-1} K^{-1})

Note:

The Evans method has a relative error of 5-10%,[7] therefore significant errors are associated with the data fitting.

Table S4: Solution χT vs T data at 5.06 X 10^{-3} M in CD_3CN solutions of *[Fe(**L**$^{Tetra\text{-}ODA}$)$(NCBH_3)_2]$*·1.5 CH_3OH measured in the heating mode from 298 to 343 ± 1 K, at 5 K intervals.

Temperature (K)	χT (cm^3. K. mol^{-1})
298	0.5082
303	0.6703
308	0.7369
313	0.8375
318	0.9859
323	1.0078
328	1.1785
333	1.382
338	1.5611
343	1.7698

7. Synthesis of complex precursors

$[Fe(Py)_4(NCBH_3)_2]\cdot 2.5H_2O$

The precursor complex used for synthesis was prepared as reported in the literature.[8] The following reaction was carried out under an inert atmosphere using Schlenk technique. Iron(II) tetrafluoroborate hexahydrate (2.00 g, 5.80 mmol, 1 eq.) and pyridine (1.82 g, 23.0 mmol, 4 eq.) were dissolved in degassed water (18 ml). To this solution sodium cyanoborohydride (0.72 g, 11.5 mmol, 2 equiv.) was added in portions. The resulting yellow suspension was stirred for one hour. The yellow solid was filtered and dried in vacuo to yield (3.288 g, 7.179 mmol Yield: 61 %) as yellow powder in moderate yields. FT-IR: $\tilde{\upsilon}$ (cm^{-1}) = 2341, 2184, 1599, 1440, 1216 , 1120, 1068, 1038, 1008, 753, 697, 626, 421. Elemental analysis calculated C, 53.17, H, 6.19, N, 16.91. Found 52.85, H, 6.00, N, 16.69.

$[Zn(Py)_4(NCBH_3)_2]\cdot 0.5H_2O$

The precursor complex used for synthesis was prepared with slight modifications to the literature.[8] Zinc(II) sulfate hydrate (2.00 g, 11.14 mmol, 1 equiv.), pyridine (3.52 g, 3.59 ml, 44.56 mmol, 4 equiv.) and sodium cyanoborohydride (1.40 g, 22.28 mmol, 2 equiv.) were suspended in water (50 ml). The reaction mixture was stirred for one hour, during which a colourless solid had formed. The solid was filtered and dried in vacuum to yield $[Zn(py)_4(NCBH_3)_2]$ as colourless powder (1.79 g, 3.87 mmol, 35 %). ^{1}H-NMR (400 MHz, DMSO, δ (ppm)): 8.58 - 8.56 (m, 8H, py*CH*), 7.82 - 7.78 (m, 4H, py*CH*), 7.41 - 7.38 (m, 8H, py*CH*), 0.56 - 0.10 (m, 6H, B*H*3) FT-IR: $\tilde{\upsilon}$ (cm^{-1}) = 2980, 2341, 2184, 1598, 1575, 1558, 1541, 1520, 1507, 1487, 1457, 1440, 1397, 1216, 1153, 1120, 1068, 1038, 1008, 860, 765, 753, 697, 626, 420. Elemental analysis calculated C, 56.16, H, 5.78, N, 17.86. Found C, 55.82, H, 5.69, N, 17.66.

8. References:

1. D. F. Evans, *J. Chem. Soc.*, 1959, 2003-2005.
2. C. Piguet, *J. Chem. Ed.*, 1997, **74**, 815-816.
3. O. Kahn, *Molecular Magnetism*, VCH Publishers Inc., New York, 1993.
4. C. P. Slichter and H. G. Drickamer, *J. Chem. Phys.*, 1972, **56**, 2142-2160.
5. H. Toftlund and J. J. McGarvey, *Top. Curr. Chem.*, 2004, **233**, 151-166.

6. L. J. Kershaw Cook, R. Kulmaczewski, R. Mohammed, S. Dudley, S. A. Barrett, M. A. Little, R. J. Deeth and M. A. Halcrow, *Angew. Chem. Int. Ed.*, 2016, **55**, 4327-4331
7. L. A. Yatsunyk and F. A. Walker, *Inorg. Chem.*, 2004, **43**, 757-77.
8. K. Nakano, N Suemura, S Kawata, A Fuyuhiro, T Yagi, S Nasu, S Morimoto and S Kaizaki, Dalton Trans., 2004, 982-988.